Molecular structure, chemical reactivity and molecular docking studies of 1,7,8,9-tetrachloro-10,10-dimethoxy-4-[3-(4-benzylpiperazine-1-yl)propyl]-4-azatricyclo[5.2.1.$0^{2,6}$] dec-8-ene-3, 5-dione.

P. K. Ranjith[a,b], C. Yohannan Panicker[c], B. Sureshkumar[d], Stevan Armakovic[e], Sanja J. Armakovic[f], C. Van Alsenoy[g], P. L. Anto[a,h]*

[a] Department of Physics, Christ College (Autonomous), Irinjalakuda, Thrissur, Kerala, India

[b] Department of Physics, MPMMSN Trusts College, Shoranur, Palakkad, Kerala, India

[c] Thushara, Neethinagar-64, Kollam, Kerala, India.

[d] Department of Chemistry, S. N. College, Kollam, Kerala, India

[e] University of Novi Sad, Faculty of Sciences, Department of Physics, Trg D. Obradovica 4, 21000 Novi Sad, Serbia

[f] University of Novi Sad, Faculty of Sciences, Department of Chemistry, Biochemistry and Environmental Protection, Trg D. Obradovica 3, 21000 Novi Sad, Serbia

[g] Department of Chemistry, University of Antwerp, Groenenborgerlaan 171, B-2020, Antwerp, Belgium

[h] Department of Physics, St. Joseph's College (Autonomous), Irinjalakuda, Thrissur, Kerala, India

* Corresponding author: email address: antoponnore367@gmail.com(P. L. Anto)

Abstract

1,7,8,9-tetrachloro-10,10-dimethoxy-4-[3-(4-benzylpiperazine-1-yl)propyl]-4-azatricyclo[5.2.1.$0^{2,6}$] dec-8-ene-3, 5-dione (TCDBPAD) have been calculated theoretically to obtain optimized geometry, vibrational frequencies and corresponding vibrational assignments. Charge transfer within the molecule was evaluated using HOMO and LUMO analysis. By hyper-conjugative interaction and charge delocalisation which can be analysed using NBO analysis, we can understand about the stability of the molecule. By using DFT method Molecular electrostatic potential (MEP) was calculated. First hyperpolarizability values are calculated in order to check

the non-linear optical activity. Using MD simulations, we have visualized the ALIE and Fukui functions. The degradation property of compound in presence of water was evaluated using RDF curves. By solubility parameter we have identified suitable excipient for the title compound. Molecular docking studies proved that the title compound can be used for the treatment of Cardiovascular and Cerebrovascular diseases.

Keywords: Azatricyclo, FT-IR, FT-Raman, DFT, ALIE, RDF, Solubility, Molecular docking.

1. Introduction

The Piperazines or cyclizines is a cyclic-organic compound that consists of a six membered ring containing two opposing nitrogen atoms. Piperazine exists as small alkaline deliquescent crystals and was introduced as a solvent for uric acid. Inside the body the drug is partly oxidized and partly eliminated unchanged. Outside the body, piperazine has an ability to dissolve uric acid and producing a soluble urate [1,2]. Piperazine derivatives used as nucleoside reverse transcriptase inhibitors for the treatment of HIV Virus [3]. Aryl piperazine derivatives exhibit a wide class of biological activities such as antiarrhythmic [4,5], anticancer [6,7], antiviral [8,9], antioxidative [10], and antibacterial [11]. Compounds of this type show high affinity for dopaminergic [12], α1-adrenergic [13], and serotoninergic receptors [14,15]. A large class of aryl piperazine derivatives of 1,7,8,9-Tetrachloro-10,10-dimethoxy-4-azatricyclo [$5.2.1.0^{2,6}$] dec-8-ene-3,5-dione were evaluated in vitro against agents of different virus classes, such as the single-stranded RNA+ viruses, Yellow Fever virus and Bovine viral diarrhoea virus, both belonging to the Flaviviridae, a HIV-1 (Retrovirus), and HBV (Hepadnavirus) [16]. Complexes of diarylpiperidin-4-one were found as the new variety of antimicrobial agents with activity against pathogenic bacterial species and fungal strains [17]. In order to analyse the effect of halogen substitution, in the parent molecule, the position of four chlorine atoms are replaced by bromine, and fluorine atoms respectively and which are designated as TCDBPAD, TCDBPAD Br and TCDBPAD F. The title compound was spectroscopically characterized by employing FT-IR and FT-Raman studies. To understand about the stability, hardness and other parameters we have calculated the HOMO-LUMO gap using DFT calculations. ALIE and Fukui functions were plotted against electron density to identify the sites of electrophilic attack. The degradation of

compound by hydrolysis was examined using the RDF curves [18]. To find out a suitable excipient we have calculated the solubility parameter by MD simulations. Thus the aim of our study was to find out the most prominent reactive sites, degradation property, suitable excipient and carrying out the docking studies.

2. Experimental Details

1,7,8,9-Tetrachloro-10,10-dimethoxy-4-azatricyclo[5.2.1.$0^{2,6}$]dec-8-ene-3,5-dione (1) was synthesized (scheme 1) as previously described [19]. 1,7,8,9-Tetrachloro-4-(3-chloropropyl)-10,10-dimethoxy-4-azatricyclo[5.2.1.$0^{2,6}$]dec-8-ene-3,5-dione (2) was prepared as follows: A mixture of imide **1** (0.5 g, 0.00138 mol), 1-bromo-3-chloropropane (0.6 g, 0.00415 mol) and anhydrous K_2CO_3 (0.5 g, 0.0036 mol) in acetonitrile (50 mL) was refluxed for 8 h. The inorganic precipitate was filtered off, the solvent was evaporated [16]. The title compound, 1,7,8,9-tetrachloro-10,10-dimethoxy-4-[3-(4-benzylpiperazine-1-yl)propyl]-4-azatricyclo[5.2.1.$0^{2,6}$] dec-8-ene-3, 5-dione (3) was prepared as follows: A mixture of compound **2** (0.3 g, 0.0007 mol), 1-benzylpiperazine (0.21 g, 0.0013 mol), anhydrous K_2CO_3 (0.3 g, 0.0022 mol) and KI (0.2 g, 0.0012 mol) was dissolved in acetonitrile (50 mL) and refluxed for 30 h. The solvent was evaporated, then the residue was purified by column chromatography (eluent: CH_2Cl_2-CH_3OH, 95:5) [16]. Yield 75%, m.p. 245.5-246 °C. Anal. Calculated: 48.06% C, 4.71% H, 7.01% N Found: 48.03% C, 4.59% H, 6.80% N.

The FT-IR spectrum (Fig.1) was recorded using KBr pellets on a DR/Jasco FT-IR 6300 spectrometer. The FT-Raman spectrum (Fig. 2) was obtained on a Bruker RFS 100/s, Germany. For excitation of the spectrum the emission of Nd:YAG laser was used, excitation wavelength 1064 nm, maximal power 150 mW, measurement on solid sample.

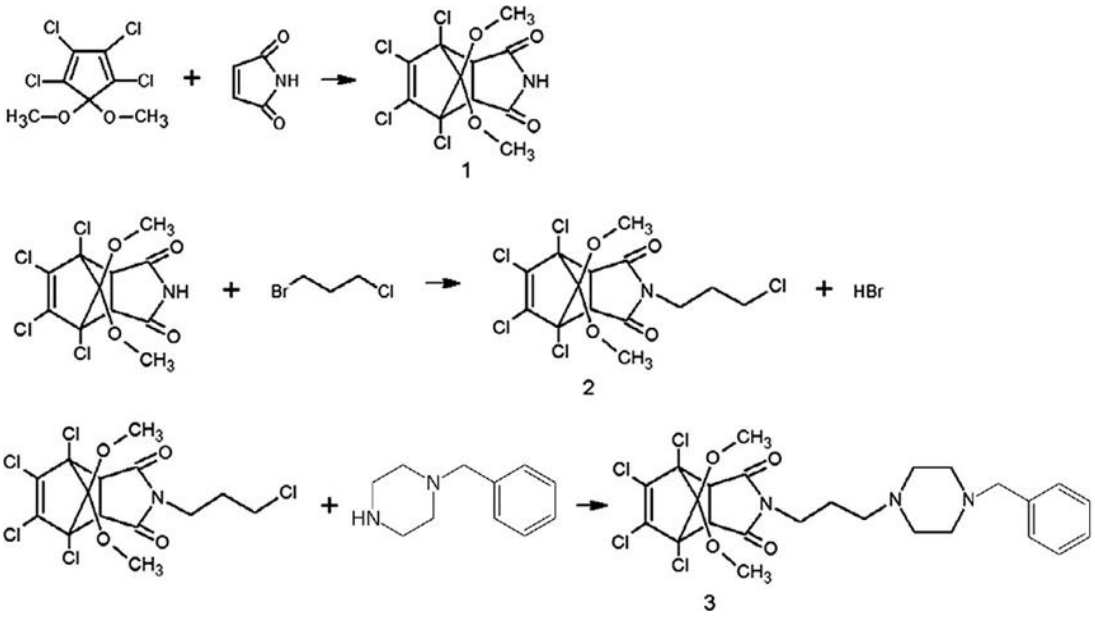

Scheme 1: Pathway of compound synthesis

3. Computational Details

Calculations of the title compound were carried with using the Gaussian09 program [20] using the B3LYP/6-31G(d') basis set to predict the molecular structure and wavenumbers in the gaseous phase and a scaling factor of 0.9613 had to be used for obtaining a considerably better agreement with the experimental data [21]. The structural parameters corresponding to the optimized geometry of the title compound (Fig. 3) are given in Table 1. The assignments of the calculated wavenumbers are done using GAR2PED [22] and Gauss view software [23]. Jaguar 9.0 and Schrodinger materials science suite 2015-4 was used for the investigation of the reactivity of the compound [24]. DFT calculations with the Jaguar were carried out using B3LYP exchange correlation functional, with 6-311++G(d,p), 6-31+G(d,p), 6-311G(d,p) basis set for the calculations of ALIE, Fukui functions and BDEs, respectively. Desmond program was used for MD simulations which was performed by OPLS 2005 force field [25], with simulation time set to 10 ns. The pressure was set at 1.0325 bar while temperature was set to 300 K. Cut-off radius was set to 12 Å, while the modelled system was of isothermal-isobaric (NPT) ensemble class. For the solvent of SPC model [26] was used here.

4. Result and Discussion

4.1 Geometrical Parameters

No data is available regarding the X-ray crystallography of the molecule, to the best our knowledge. Moreover, the reported structural parameters of the parental molecule significantly correlate with our theoretical predictions attesting the authenticity of our results.

In the following discussion, the cyclohexene ring is designated as RI, the imido fragment ring is designated as RII, piperazine ring is designated as RIII, Phenyl ring is designated as RIV.

The bond angles of imido fragment of title compound give theoretically as C_{16}-N_{15}-C_{13} = 114.0, O_{18}-C_{13}-N_{15} = 124.6, O_{18}-C_{13}-C_4 = 127.4, N_{15}-C_{13}-C_4 = 107.9, C_{13}-C_4-C_5 = 105.0, C_{13}-C_4-H_{10} = 107.3, C_5-C_4-H_{10} = 114.2, C_{16}-C_5-H_{12} = 107.6, C_4-C_5-H_{12} = 114.1, O_{17}-C_{16}-N_{15} = 124.7, O_{17}-C_{16}-C_5 = 127.3, N_{15}-C_{16}-C_5 = 107.9° respectively, whereas the reported values of similar derivatives are 114.7, 124.0, 128.5, 107.4,105.8, 112.3, 113.8, 113.3, 113.1, 126.3, 129.2, 106.5° and 111.0, 126.1, 128.4, 105.5,109.9, 115.0, 136.0, 118.0, 118.0, 123.7, 131.4, 104.9° [27]. Conley et al. [27] reported the dihedral angles, C_{16}-N_{15}-C_{13}-O_{18} = 179.5, C_{16}-N_{15}-C_{13}-C_4 = 4.0, O_{18}-C_{13}-C_4-C_5 = 177.5, N_{15}-C_{13}-C_4-C_5 = 0.5, C_{13}-C_4-C_5-C_{16} = 1.7, C_{13}-N_{15}-C_{16}-C_5 = 5.1, C_4-C_5-C_{16}-O_{17} = 176.7, C_4-C_5-C_{16}-N_{15} = 4.0° whereas for the title compound the corresponding values are 177.3, 6.7, 177.6, 1.7, 3.1, 8.8, 176.5 and 7.0° respectively. Pinho e Melo et al. [28] reported the bond lengths N_{15}-C_{16} = 1.3654, N_{15}-C_{13} = 1.4484 Å, bond angles C_{16}-N_{15}-C_{13} = 116.8, C_{16}-N_{15}-C_{19} = 121.6, C_{13}-N_{15}-C_{19} = 121.6, C_5-C_{16}-N_{15} = 121.9, N_{15}-C_{13}-C_4 = 107° which are in agreement with our calculated values. Lee and Swager [29] reported the bond lengths C_{16}-O_{17} = 1.1954, C_{13}-O_{18} = 1.2054, N_{15}-C_{16} = 1.3776, C_{13}-N_{15} = 1.3765 Å and the bond angles C_5-C_{16}-N_{15} = 106.3, C_4-C_{13}-N_{15} = 106.5°. The B3LYP calculations give the bond lengths within the imido fragment as C_{16}-O_{17} = 1.2095, C_{13}-O_{18} = 1.2077, N_{15}-C_{16} = 1.3917, C_{13}-N_{15} = 1.3933, C_{13}-C_4 = 1.5337, C_{16}-C_5 = 1.5373, C_5-C_4 = 1.5534 Å and bond angles C_5-C_{16}-N_{15} = 107.9, C_4-C_{13}-N_{15} = 107.9°. Conley et al. [27] reported the corresponding values as 1.2025, 1.3985, 1.2104, 1.4054, 1.4865, 1.5155, 1.555 Å and 1.1974, 1.3995, 1.2004, 1.3824, 1.4866, 1.4826, 1.3436 Å for different similar derivatives. The N_{15}-C_{19} bond length (1.4617 Å) is longer than N_{15}-C_{13} (1.3933 Å) and N_{15}-C_{16} (1.3917 Å) bond lengths. This indicates, as expected, a delocalized p-

electron system along the imide part of the molecule (O_{18}-C_{13}-N_{15}-C_{16}-O_{17}) as reported by Bartkowska et al. [30]. Berendsen et al. [26] reported the bond lengths, C_{13}-O_{18} = 1.2032, N_{15}-C_{13} = 1.3913, C_{13}-C_4 = 1.5193, C_4-C_5 = 1.5453, C_{16}-O_{17} = 1.2073, N_{15}-C_{16} = 1.3880 Å and the bond angles, N_{15}-C_{19}-C_{28} = 111.3, O_{18}-C_{13}-N_{15} = 124.3, O_{18}-C_{13}-C_4 = 127.8, N_{15}-C_{13}-C_4 = 107.8, O_{17}-C_{16}-N_{15} = 127.2, N_{15}-C_{16}-C_5 = 107.0, C_{16}-N_{15}-C_{13} = 114.2, C_{16}-N_{15}-C_{19} = 123.8 and C_{13}-N_{15}-C_{19} = 121.7° whereas the corresponding values in the present case are 1.2077, 1.3933, 1.5337,1.5534, 1.2095, 1.3917 Å and 113.0, 124.6, 127.4, 107.9,124.7,107.9, 114.0, 123.3, 122.4°. For the title compound the C_4-H_{10}, C_5-H_{12} bond lengths are 1.0945, 1.0948 Å respectively, whereas reported values are 0.9600, 0.9601 Å [27]. The cyclohexene ring fragment is a sterically strained system. Presumably, this is the reason for elongation of skeletal CC bonds, C_1-C_2, C_2-C_3, C_3-C_4, C_5-C_6, and C_6-C_1. The CC bond lengths in the five member ring (C_5-C_{16}, C_4-C_{13}) are elongated to a lesser extent. These may be explained by change of the substitution pattern in the nitrogen containing five member rings as reported by Tarabara et al. [31]. The methoxy groups, O_{14}-C_{11}-H_{23}, $_{24}$, $_{27}$ and O_9-C_8-H_{20}, $_{21}$, $_{22}$ inclined almost equally with respect to the other parts of the six member ring. The bond angles C_1-C_6-C_7, C_5-C_6-C_7, C_2-C_3-C_7, C_4-C_3-C_7, C_6-C_1-C_2 and C_4-C_3-C_2 are respectively 99.5, 102.3, 99.6, 102.8, 107.9 and 104.7°. In addition, the declination of the five member ring from the cyclohexene ring are given by the angles C_6-C_5-C_{16} and C_3-C_4-C_{13} by 118.2 and 118.8° which are almost equal as reported in the literature [31]. The conjugation in the imido group is essentially disturbed; the torsion angles C_{13}-N_{15}-C_{16}-C_5, C_{16}-N_{15}-C_{13}-C_4 are 8.8, -6.7° and the C_{13}-$N_{15}$and C_{16}-N_{15} bond lengths are elongated to 1.3933, 1.3917 Å relative to the average value 1.3925 Å [32]. For the cyclohexene ring, Manohar et al. [33] reported the bond lengths C_1-C_2 = 1.3194, C_1-C_6 = 1.5174, C_6-C_5 = 1.5523, C_6-C_7 = 1.5484, C_5-C_4 = 1.5353, C_4-C_3 = 1.5543, C_3-C_7 = 1.5473, C_3-C_2 = 1.5144 Å and the corresponding bond lengths of the title compound are 1.3421, 1.5304, 1.5638, 1.5810, 1.5534, 1.5711, 1.5854, 1.5265 Å. The bond angles reported by Manohar et al. [33] are C_3-C_4-C_5 = 102.9, C_3-C_2-C_1 = 107.5, C_3-C_7-C_6 = 92.4, C_2-C_3-C_4 = 107.2, C_6-C_5-C_4 = 103.1, C_6-C_1-C_2 = 107.7, C_5-C_6-C_1 = 106.8, C_2-C_3-C_7 = 99.52, C_4-C_3-C_7 = 101.1, C_5-C_6-C_7 = 101.1, C_1-C_6-C_7 = 99.4Å whereas the corresponding calculated (DFT) values of the title compound are 103.1, 107.3 91.4, 104.7, 103.1, 107.9, 105.7, 99.6, 102.8, 102.3, 99.5°. In the present case, the oxygen atoms O_{17} and O_{18} are equally inclined from the N_{15} atom given by the angles O_{17}-C_{16}-N_{15}, O_{18}-C_{13}-N_{15} (124.6°) and from C_4 and C_5 atoms given by the angles O_{17}-C_{16}-C_5, O_{18}-C_{13}-C_4 (127.3°) as reported in the literature [34].

There are four types of CC bonds involved in the title compound, strained CC bonds of R1, RII, RIII, RIV, propyl group and of the carbon-carbon bridge. The CC bond lengths are in the range 1.5265-1.5711, 1.5337-1.5534 and 1.5340,1.5342 Å, in R1, RII, propyl group, 1.5854, 1.5810 Å in the carbon-carbon bridge and 1.5255 in benzyl fragment respectively. The CH bond lengths are calculated as C_4-H_{10} = 1.0945 and C_5-H_{12} = 1.0948 Å. The CH bond lengths are in the range 1.0950-1.1126 Å for the bridging CH_2 groups, and for the CH_3 groups, CH bond lengths are in the range of 1.0931-1.0957 Å. The optimized carbon-carbon bridge angles C_3-C_7-C_6 = 91.4° is similar to the structures reported by Manohar et al. [33]. The propyl group is tilted from the RII, as is evident from torsion angles, C_5-C_{16}-N_{15}-C_{19} (177.1°), C_{16}-N_{15}-C_{19}-C_{28} (92.2°), C_4-C_{13}-N_{15}-C_{19} (179.2°) and C_{13}-N_{15}-C_{19}-C_{28} (81.5°). The double bonds C_{16}-O_{17} and C_{13}-O_{18} are conjugated with the p-system of the RII, with the torsion angles O_{17}-C_{16}-N_{15}-C_{13}, C_{16}-N_{15}-C_{13}-C_4 being 174.6, 6.7° and O_{18}-C_{13}-N_{15}-C_{16}, C_{13}-N_{15}-C_{16}-C_5 being 177.3, 8.8° respectively as reported by Kasyan et al. [35]. At N_{15} position, the bond angles C_{16}-N_{15}-C_{19} = 123.3, C_{13}-N_{15}-C_{19} = 122.4 and C_{16}-N_{15}-C_{13} = 114.0° and this asymmetry of angles reveal the steric repulsion of the atoms H_{26}, H_{25} and O_{17}, O_{18} [35]. For the piperazine ring, El-Emam et al. [36] reported the bond lengths N_{38}-C_{40} = 1.4650, N_{38}-C_{39} = 1.4630, C_{39}-C_{46} = 1.5140, N_{47}-C_{45} = 1.4580, N_{47}-C_{46} = 1.4710, C_{40}-C_{45} = 1.5110 Ǻ and the corresponding bond lengths of the title compound are 1.4714, 1.4574, 1.5400, 1.4540, 1.4646, 1.5438 Å respectively. The DFT calculations give the bond angles within the piperazine ring N_{38}-C_{39}-C_{46} = 110.2, N_{38}-C_{40}-C_{45} = 111.6, N_{47}-C_{45}-C_{40} = 109.5, N_{47}-C_{46}-C_{39} = 110.8, C_{45}-N_{47}-C_{46} = 112.3°. El-Emam et al. [36] reported the corresponding values as 110.0, 109.7, 109.7, 110.0 and 110.0° for different similar derivatives. Gao et al. [37] reported the dihedral angles C_{40}-N_{38}-C_{39}-C_{46} = 55.3, C_{45}-N_{47}-C_{46}-C_{39} = 57.6, N_{38}-C_{39}-C_{46}-N_{47} = 56.3, C_{46}-N_{47}-C_{45}-C_{40} = 57.7, C_{39}-N_{38}-C_{40}-C_{45} = 55.3, N_{47}-C_{45}-C_{40}-N_{38} = 55.9° which are in agreement with our calculated values.

4.2 IR and Raman Spectra

The calculated (scaled) wavenumbers observed IR, Raman bands and assignments are given in Table. 2. The assignments of the benzene ring vibrations are made by referring [38] the case of benzene derivatives with mono substitution as summarized by Roeges. According to Roeges, the CH stretching modes for mono substituted benzene are found in the region 3105-3000 cm^{-1} [38].

For the title compound, the bands observed at 3069 cm^{-1} in the IR spectrum and 3068, 3053 cm^{-1} in the Raman spectrum are assigned as CH stretching mode of the phenyl ring. The calculated (DFT) values are at 3078, 3066, 3058, 3046 and 3044 cm^{-1} [38]. The bands observed at 1621, 1477, 1438 and 1307 cm^{-1} in the IR spectrum and at 1610 and 1573 cm^{-1} in the Raman spectrum are assigned as νIV ring stretching modes. Theoretically these modes are assigned at 1598, 1579, 1479, 1437 and 1309 cm^{-1}. These vibrations are expected in the region 1620-1300 cm^{-1} [38]. For the title compound, the ring breathing mode of phenyl ring is found at 979 cm^{-1} theoretically [38]. The bands observed at 1140, 1065 cm^{-1} in the IR spectrum and 1161, 1014 cm^{-1} in the Raman spectrum are assigned as the in-plane bending vibrations of CH modes of phenyl ring. DFT calculations give these modes at 1164, 1161, 1140, 1068 and 1016 cm^{-1}. For the title compound, the bands at 921, 891, 828 cm^{-1} in the IR spectrum and 930, 893, 824, 735 cm^{-1} in the Raman spectrum are assigned as the out-of-plane CH deformations of the phenyl ring. The γCH bands are found theoretically at 950, 924, 893, 828 and 731 cm^{-1}. In aromatic methoxy compounds, $\upsilon_{as}CH_3$ bands are expected in the region [38] 2985 ± 20 and 2955 ± 20 cm^{-1} and the symmetrical stretching mode υ_sCH_3 is expected in the range 2845 ± 45 cm^{-1} in which all the three CH bonds extend and contract in phase [38]. For the title compound, corresponding calculated wavenumbers are at 3048, 3035, 3034, 3019 cm^{-1} as υ_aCH_3 and 2952, 2941 $cm^{-1}$for υ_sCH_3 vibrations. Experimentally $\upsilon_{as}CH_3$ band is assigned at 3030 cm^{-1}. With methyl esters the overlap of the regions in methyl asymmetrical deformations are active (1465 ± 10 and 1460 ± 15 cm^{-1}) and is quite strong, which leads to many coinciding wavenumbers [38]. This is obvious, not only for the asymmetric deformation, but also for the symmetric deformation [38] mostly displayed in the range 1450 ± 20 cm^{-1}. The intensity of these absorptions is only weak to moderate. The DFT calculations give the deformation modes of CH_3 at 1474, 1465, 1459, 1453, 1437, 1422 cm^{-1} for the title compound. The bands observed at 1453, 1418 cm^{-1} in the Raman spectrum are assigned as the deformation bands of the methyl group. The methyl rocking vibration [38] are expected at 1190 ± 45 cm^{-1}. The second methyl rock [38] absorb at 1150 ± 30 cm^{-1}. The bands at 1191, 1178, and 1133 cm^{-1} theoretically were assigned as rocking modes of the methyl group. These modes are observed at 1178 cm^{-1} in the IR spectrum. Methoxy groups attached to an aromatic ring give CO stretching modes in the range 1200-900 cm^{-1} [39]. The DFT calculation gives CO stretching vibrations at 1167, 1143, 1091, 1031, 1005, 989, 970 and 947 cm^{-1}. The bands observed at 1087, 1004, 969, 943 cm^{-1} in the IR spectrum and at 1088, 997,

973, 948 cm^{-1} in the Raman spectrum are assigned as νCO stretching vibrations. Renjith et al. [40] reported the asymmetric and symmetric νCO stretching vibrations in the range 1145, 1065 cm^{-1} and 961-947 cm^{-1}. Castaneda et al. reported the methoxy vibrations at 1252, 1190, 1172, 1028 and 1011 cm^{-1} [41]. The C=O stretching frequency appears strongly in the IR spectrum in the range 1600-1700 cm^{-1} because of its large change in dipole moment. The carbonyl group vibrations give rise to characteristics bands in vibration spectra and its characteristic frequency used to study a wide range of compounds. The intensity of these bands can increase owing to conjugation or formation of hydrogen bonds [42,43]. The carbonyl band of cyclic imides is shifted to higher wavenumber if the ring is strained [43]. The carbonyl groups in the imide fragment give rise to bands [43,44] in the region of 1790-1720 $cm^{-1.}$ For the title compound, the C=O stretching bands are observed at 1766, 1698 cm^{-1} in the IR spectrum, 1788, 1727 cm^{-1} in the Raman spectrum and at 1786, 1728 cm^{-1} theoretically (DFT). The CC vibrations in RI and RII are calculated at 1135, 1100 and 1052 cm^{-1} theoretically and in between 1137-1054 cm^{-1}experimentally. Renjith et al. reported these values in between 1093-962 cm^{-1} theoretically, at 1011, 999, 964 cm^{-1} in the Raman spectrum [40]. The CN stretching modes are reported [45] in the range 1300-1100 cm^{-1}. Silverstein et al. assigned CN stretching absorption in the region 1382-1266 cm^{-1} for aromatic amines [46]. In the present case, the νCN stretching modes to C_{13}-N_{15}, C_{16}-N_{15}, C_{19}-N_{15}, C_{31}-N_{38} and C_{63}-N_{47} are observed at 1347, 1151, 1121 cm^{-1} in the IR spectrum 1340, 1121 cm^{-1} in the Raman spectrum and at 1348, 1339, 1144, 1127, 1107 cm^{-1} theoretically. Kasyan reported the CN stretching in the region 1350-1100 cm^{-1} [47]. For bridging methylene groups, the CH_2 (at C_{19}, C_{28}, C_{31}, C_{63}) vibrations are observed in the region of 3000-2800, 1400-1200, 1150-875 and 850-600 cm^{-1} [48]. The vibrations of these CH_2 groups (the asymmetric stretch $\upsilon_a CH_2$, symmetric stretch $\upsilon_s CH_2$, the scissoring vibration and wagging vibration) appear in the regions of 3005-2940, 2940-2870, 1480-1420 and 1380-1320 cm^{-1} respectively [38,39,49]. These bands are observed at 2989, 2954, 2781 cm^{-1} in the IR spectrum, 3016, 2988, 2961, 2792 cm^{-1} in the Raman spectrum and at 3018, 2991, 2962, 2953, 2947, 2930, 2910, 2782 cm^{-1} theoretically (DFT) for the title compound respectively. According to literature [46] scissoring mode of the CH_2 group give rise to characteristic band near 1465 cm^{-1} in IR and Raman spectra. These modes are unambiguously correlated with the strong bands in the region of 1449-1376 cm^{-1} observed experimentally and theoretically these bands are assigned in between 1464-1378 cm^{-1}. The twisting and rocking vibrations of the CH_2 group appear in the

region [39] of 1280-1200 and 900-740 cm^{-1} respectively. These modes are also assigned (Table 2). For the title compound these deformation modes are observed in the range 1298-716 cm^{-1} theoretically and are observed at 1246, 845, 799, 746 cm^{-1} in the IR spectrum, 1297, 1280, 1252, 1235, 835, 754 cm^{-1}in the Raman spectrum. These modes are not pure, but contain significant contributions from other modes also. In the bridging methylene group (C_{19}-C_{28}, C_{28}-C_{31} and C_{63}-C_{52}) CC stretching modes are found at 1169, 1035, 1009 cm^{-1} theoretically and at 1035, 1010 cm^{-1} in the IR spectrum. The CH stretching vibrations occur [39] above 2900 cm^{-1} and CH deformations absorb weakly in the region of 1350-1315 cm^{-1} in the infrared and more distinctive in Raman spectrum. For the title compound the DFT calculations give the υCH modes in RI at 2991 and 2983 cm^{-1}. Kasyan et al. and Tarabara et al. reported the υCH modes at 3080 cm^{-1} and 3070-3050 cm^{-1} for similar derivatives [47,31]. Most of the bands are not pure, but contains significant contributions from other modes. The C=C stretching mode is expected in the region [48] 1667-1640 cm^{-1}. For the title compound, the C=C stretching mode is assigned at 1595 cm^{-1} in the Raman spectrum and at 1597 cm^{-1} theoretically. For a series of propenoic acid esters, Felfoldi et al. reported the υC=C at 1625 cm^{-1} [49] theoretically. The deformation modes in RI are observed at 1270, 1261, 1226, 1192 (DFT), 1270, 1194 cm^{-1}(IR) and at 1265, 1194 cm^{-1}(Raman). The vibrations belonging to the bond between the ring and chlorine atoms are worth to discuss here since mixing of vibrations is possible due to the lowering of the molecular symmetry and the presence of heavy atoms on the periphery of the molecule [50-52]. Mooney assigned vibrations of CCl, CBr and CI in the wavenumber range of 1129-480 cm^{-1} [51,52]. The CCl stretching vibrations give generally strong bands in the region 710-505 cm^{-1}. For simple organic chlorine compounds, CCl absorptions are in the region 750-700 cm^{-1}. Sundaraganesan et al. reported CCl stretching at 704 (IR), 705 (Raman) and 715 cm^{-1} (DFT) and the deformation bands at 250 and 160 cm^{-1} [53]. The aliphatic CCl bands absorb [34] at 830-560 cm^{-1} and putting more than one chlorine on a carbon atom raises the CCl wavenumber. The CCl stretching mode is reported at around 738 cm^{-1} for dichloromethane and scissoring mode δCCl at around 284 cm^{-1} [54,39]. Pazdera et al. reported the CCl stretching mode at 890 cm^{-1} [55]. For 2-cyanophenylisocyanide dichloride, the CCl stretching mode is reported at 870 (IR), 877 cm^{-1} (Raman), and 882 cm^{-1} theoretically [56]. Arslan et al. reported the CCl stretching mode at 683 (experimental) and at 736, 711, 697 and 687 cm^{-1} theoretically [57]. The deformation bands of CCl are reported [56] at 441, 435 and 431 cm^{-1}. For the title compound the bands at 668, 616 cm^{-}

^{1} in Raman and 700, 657 and 610 (DFT) are assigned as CCl stretching modes. The asymmetric stretching CH_2 vibrations in the piperazine ring is reported in the range 3033-2966 cm^{-1}, while the symmetric vibrations lying in the range 2874-2834 cm^{-1} [36]. For the title compound, the bands observed at 2963, 2958, 2935, 2917, 2857, 2837, 2817, 2804 cm^{-1} (DFT) are assigned for CH_2 stretching modes. These bands are observed at 2878, 2837 cm^{-1}in the IR spectrum and 2959, 2832, 2817, 2805 cm^{-1}in the Raman spectrum. In a study on the determination of piperazine rings in ethylene amines, poly (ethyleneamine) and polyethylenimine by infrared spectrometry, Spell reported that the piperazine ring was found to be associated with sharp, well defined absorptions at 1345-1300 cm^{-1}, 1170-1125 cm^{-1}, 1025-1010 cm^{-1} and 940-915- cm^{-1} regions of the IR spectrum [58]. El-Emam et al. reported the vibrations of CH_2 groups in the piperazine ring (the asymmetric stretch $\upsilon_a CH_2$, symmetric stretch $\upsilon_s CH_2$, the scissoring vibration and wagging vibration) in the range 3033-2966, 2874-2834, 1457-1422 and 1379-1344 cm^{-1}respectively [36]. As stated by Spell, this is one of the most useful bands for detecting the presence of di-substituted piperazines [58]. The twisting and rocking vibrations of the CH_2 group appear in the region [39] of 1280-1200 and 900-740 cm^{-1} respectively. These modes are also assigned (Table 2). For the title compound the deformation modes are observed at in the range 1473-860 cm^{-1} theoretically, at 1402, 1378, 1229, 1212 cm^{-1}(IR) and at 1473, 1402, 1376, 1357, 1321, 1211, 1071, 1044, 860 cm^{-1}(Raman). These modes are not pure, but contain significant contributions from other modes also. El-Emam et al. reported the CN stretching vibrations in the region 1154-756 cm^{-1} [36]. For the title compound (C_{40}-N_{38}, C_{39}-N_{38}, C_{45}-N_{47}, C_{46}-N_{47}) CN stretching vibrations (in RIII) are found at 1188, 1116, 954, 804, 788, 764 cm^{-1} theoretically. Experimentally these modes are assigned at 805,785,778, 771 cm^{-1}. The shift in the wavenumber may be attributed to the bulky groups attached to the piperazine ring. The CC stretching vibrations for the title compound in RIII are observed at 986, 960, 895 cm^{-1} theoretically, and at 987 cm^{-1} experimentally. These vibrations in the piperazine ring were reported at 972, 903 cm^{-1} [36].

4.3 Frontier Molecular Orbital

Frontier molecular study is used to explain the chemical behaviour and stability of molecular system. The atomic orbital components of the frontier molecular orbital are shown in Fig. 4. The

delocalization of HOMO and LUMO over the molecular system shows the charge transfer with in the molecular system. The HOMO-LUMO gap is found to be 3.144 eV. The chemical description can be evaluated by using HOMO-LUMO orbital energies, E_{HOMO} and E_{LUMO} as: ionisation energy $I = -E_{HOMO}$, electron affinity $A = -E_{LUMO}$, chemical hardness $\eta = (I-A)/2$, chemical potential $\mu = -(I+A)/2$ and electrophilicity index ($\omega = \mu^2/2\eta$) [59]. For the title compound I = 8.087, A = 4.943, η = 1.572, μ = -6.515, ω = 13.500 eV (Table. 3). For the title compound, HOMO is delocalized over cyclohexene ring, partially over imido fragment while the LUMO is delocalized strongly over the phenyl ring and partially over the piperazine ring. For fluorine substitution HOMO is delocalized strongly over cyclohexene, piperazine rings and partially over the bridge CH_2 while LUMO is deeply over phenyl ring and N_{47} atom of piperazine ring. For halogen bromine substitution HOMO is delocalized strongly over cyclohexene ring while LUMO is delocalized strongly over phenyl ring. The chemical potential decreases for halogen substitution in the order of bromine substitution< fluorine substitution< parent molecule. The electrophilicity index decreases for halogen substitution in the order fluorine substitution < parent molecule < bromine substitution.

4.4 Molecular Electrostatic Potential Map

Molecular electrostatic potential and electron density are associated to each other to find the reactive sites for electrophilic and nucleophilic sites [60,61]. For the parent molecule most electrophilic (red and yellow) regions of MEP map (Fig. 5) were related electrophilic reactivity while positive blue regions to nucleophilic reactivity. For the parent molecule the electrophilic regions are deeply over N_{38} atom of piperazine ring, slightly over the phenyl ring, marginally over the carbon atoms of cyclohexene ring, slightly over oxygen atoms of imido fragment. The nucleophilic region (blue) is deeply over the hydrogen atoms in the phenyl ring and strongly over methoxy group of cyclohexene ring and deeply over the chlorine atoms of parent molecule.
For fluorine substitution electrophilic region is deeply over the N_{38} atom in the piperazine ring, very slightly over carbon atoms in the phenyl ring (C_{55}, C_{59}). The electrophilic region of carbon atoms in the cyclohexene ring is slightly greater than parent molecule. The nucleophilic region of fluorine substitution is deeply over fluorine atoms and CH_2 groups of propyl part of the molecule. The other part of nucleophilic region of TCDBPAD fluorine is almost same as that of

parent molecule. For halogen substitution bromine atom, the electrophilic region is strongly over the N_{38} atom in the piperazine ring, slightly over carbon atoms in the cyclohexene ring but greater than that of TCDBPAD fluorine. Nucleophilic region is maximum pronounced over the methoxy group, bromine atoms and phenyl ring. Electrophilic region of phenyl ring of parent molecule > TCDBPAD fluorine > TCDBPAD bromine. Nucleophilic region is same for halogen atoms in parent molecule and fluorine substitutions but greater than bromine substitutions. The electrophilic region in the piperazine ring is same for three halogen substitutions. The electrophilic region of cyclohexene ring is more pronounced in bromine substitution than parent molecule and fluorine substitutions.

4.5 Natural Bond Orbital Analysis

The NBO (Natural Bond Orbitals) calculations were executed using NBO 3.1 program [62]. The strong interactions are: $LPN_{15}\rightarrow C_{13}\text{-}O_{18}$, $LPN_{15}\rightarrow C_{16}\text{-}O_{17}$, $LPO_{17}\rightarrow C_{5}\text{-}C_{16}$, $LPO_{17}\rightarrow N_{15}\text{-}C_{16}$, $LPO_{18}\rightarrow C_{4}\text{-}C_{13}$, $LPO_{18}\rightarrow C_{13}\text{-}N_{15}$, $LPCl_{35}\rightarrow C_{2}\text{-}C_{3}$ and $LPCl_{36}\rightarrow C_{1}\text{-}C_{2}$ with energies, 50.47, 51.78, 20.16, 25.63, 20.01, 25.99, 14.68 and14.97 kcal/mol. 100% p-character is found in lone pairs of O_9, O_{14}, N_{15}, O_{17}, O_{18}, Cl_{34}, Cl_{35}, Cl_{36} and Cl_{37} atoms. The significant results are tabulated in Tables 4 and 5.

4.6 First Hyperpolarizability

Organic molecules able to control photonic signals efficiently and are of importance in technologies such as optical communication, optical computing and dynamic image processing. The calculated first hyperpolarizability of the 1,7,8,9 - Tetrachloro-10,10-dimethoxy-4-[3-(4-benzylpiperazin-1-yl)propyl]-4-azatricyclo[5.2.1.$0^{2.6}$] dec-8-ene-3,5-dione is 1.6690 X 10^{-30} esu which is 12.84 times that of the standard NLO material urea (0.13 x 10^{-30} esu) [63]. Which is comparable with the reported values of similar derivatives (11.77 times that of urea) [64]. From this value we can say that the title compound is an attractive object for future nonlinear studies. In the halogen substituted NLO study of the title compound showed that the hyperpolarizability increases to 2.4111 x 10^{-30} esu for fluorine substitution and 1.7503 x 10^{-30} esu for bromine substitution in the place of chlorine atoms in the title compound (Table 6).

4.7 ALIE surfaces and Fukui functions

The local reactivity and the energy required to remove an electron from a molecule are explained using the quantum molecular descriptor ALIE (Average local ionization energy) sjoberg et.al. defined that ALIE consists sum of orbital energies [65]. According to this we can say that the sites with least values of ALIE are the most probable sites for an electrophilic attack [66]. The equation of ALIE is the sum of orbital energies weighted by the orbital density.

$$I(r)=\sum_i \frac{\rho_i(\vec{r})|\varepsilon_i|}{\rho(\vec{r})}$$

Where $\rho_i(\vec{r})$ denotes electronic density of the i-th molecular orbital at the point $\vec{r}$, ε_i denotes orbital energy and $\rho(\vec{r})$ denotes total electronic density function. We have mapped the ALIE values to the electron density surface in order to foresee the attacking sites of electrophiles. The ALIE figure is represented in Fig. 6. Here in this figure we can see that the two nitrogen atoms show the least ALIE values that is 167.81 kcal/mol, while the hydrogen atom shows the highest ALIE value 332.15 kcal/mol. Fukui functions are very useful in determining the local reactive sites in a molecule. The functional derivative of chemical potential with respect to external potential is termed as Fukui functions. This quantum molecular descriptor is interpreted as the derivative of electronic density with respect to the number of electrons [67-69]. In physical sense it is the change in electron density as a consequence of change in charge. These functions in Jaguar program are calculated with the help of finite difference approach, according to the following equations:

$$f^+ = \frac{\left(\rho^{N+\delta}(r)-\rho^N(r)\right)}{\delta},$$

$$f^- = \frac{\left(\rho^{N-\delta}(r)-\rho^N(r)\right)}{\delta},$$

where *N* stands for the number of electrons in reference state of the molecule, while δ stands for the fraction of electron which default value is set to be 0.01 [69] . By plotting Fukui functions to

electron density surfaces we get all information's about the important reactive centres [65,66]. The Fukui function plot is represented in Fig. 7. The colour coding in the plot is as follows, purple (positive) colour in Fukui function f^+ means the electron density has been increased by the addition of charges to the system while red (negative) color in Fukui function f^- means the electron density has been diminished by the addition of charges. Electron density is increased in the near vicinity of carbon atoms C_{28}, C_{31} and electron density is decreased near the O_{18}, O_{17} atom.

4.8 Degradation properties based on autoxidation and hydrolysis

RDF is calculated to predict degradation properties based on autoxidation and hydrolysis mechanisms. To find the extend of hydrolysis we have calculated the RDF for the molecule. In Fig.8 RDFs of atoms with the most pronounced interactions with water molecules are presented. In RDF plot, g(r) represents the probability of finding a particle in the distance r from another particle [70]. Results provided in Fig.8 indicate that only five atoms of TCDBPAD molecule have relatively significant interactions with water molecules. These are oxygen and nitrogen atoms O_9, O_{17}, O_{18}, N_{38} and N_{47}. Peak distance in all cases is located between 2.7 to 3 Å. According to the maximal g(r) values the most important RDF is certainly for O_{18} atom. In pharmaceutical industry stability of molecule near water sorroundings, relatively high peak and absence of hydrogen atoms in the peak is very much relevant.

4.9 Hildebrand solubility parameter -Identification of excipients

The emerging field in pharmaceutical is the production of new products and the identification of the active ingredient. To be considered for drug production there are certain parameters. Some of them are the solubility, stability and deliverability of the active ingredient. Modifications are done to the molecules which lack these parameters. Without any structural changes we can modify the molecule by intermixing them with the excipient. Wide range of excipients are identified over the time. Excipients can be identified using computational methods as well as experimental methods. Experimental identification is a laborious process, while computational methods are uncomplicated and effortless. Compatibility is the major property needed between

the active ingredient and the excipient. Hildebrand solubility parameter can be used to predict the compatible nature of excipient and the ingredient [71-73]. The solubility parameter of active component and that of the excipient must be same. The equation for the Hildebrand solubility parameter using MD calculations is given below

$$\delta = \sqrt{\frac{\Delta H_V - RT}{V_m}} \quad (1)$$

In this work, the solubility parameter has been calculated for the TCDBPAD molecule. Its value has been compared with the common excipient compounds polyvinylpyrrolidone polymer (PVP), maltose, and sorbitol. MD systems used to calculate this quantity consisted of 32 molecules placed in a cubic simulation box. Solubility parameters of all mentioned compounds have been summarized in Table. 7. As indicated by the results presented in Table. 7, TCDBPAD molecule has the highest compatibility with the PVP compound. In this particular case, the difference between corresponding values of solubility parameter is less than 0.5 $MPa^{1/2}$, indicating very high compatibility. Solubility parameters of sorbitol and maltose is much higher than the solubility parameter of the TCDBPAD molecule. Therefore, the MD calculations suggest that it is reasonable to consider PVP as an excipient for TCDBPAD molecule.

4.10 Molecular Docking

Molecular docking tries to predict the structure of intermolecular complex formed between two or more constituent molecules. The final goal uses to be to predict the biological activity of a given ligand. Molecular docking was employed to recognize the active site of the receptor and acquire the best geometry of ligand-receptor complex. Based on the structure of the title compound, we find the activity of non-basic fXa inhibitors with excellent potency in anti-fXa and anticoagulant assays. Among the many enzymes in the coagulation cascade, factor fXa is one particularly attractive target [74]. Cardiovascular and cerebrovascular diseases, such as deep venous thrombosis (DVT), myocardial infarction (MI), pulmonary embolism (PE), and ischemic stroke, are now and may continue to be leading causes of morbidity and mortality around the world [74]. Factor Xa (PDB ID: 1wu1) was downloaded from the RCSB protein data bank website. Although thrombin is one of the adequate targets for anticoagulation, there are a few

reports in which direct factor Xa (fXa) inhibitors decrease the likelihood of bleeding tendency compared with direct thrombin inhibitors [75-77]. The structure of a large molecular fragment of factor Xa that lacks only a Gla domain has been solved by x-ray crystallography and refined at 2.2A resolution of crystallographic R value of 0.168 [78]. Among several approaches to address the unmet needs, the inhibition of factor Xa (fXa) is known as one of the most popular. This is mainly because fXa inhibitors seemed to have a lower risk of bleeding than heparin and warfarin. The reason would be attributed to the inhibition position in the coagulation cascade. As is well-known, fXa catalyzes thrombin production and is situated at the confluence of the intrinsic and extrinsic pathways. Thus, fXa inhibitors do not block thrombin directly rather, they block the confluent position of the coagulation cascade [79]. Thus, we choose title compound as ligand and Factor Xa receptor as target for docking study. All molecular docking calculations were performed on AutoDock 4.2 [80] and AutoDock Vina software [81]. The original ligand as well as water molecules were removed from the crystal structure, and polar hydrogens and united atom Kollman charges were assigned for the receptor using the graphical user interface AutoDock Tools (ADT). The Lamarckian Genetic Algorithm (LGA) [82] was employed to calculate the energy between ligand and receptor. The compound docked the active site of receptors with the grid centre dimension 40×40×40. The conformations with the lowest binding energy is extracted and analysed for detailed interactions in Discovery Studio Visualizer 4.0 software. The ligand binds at the active site of the substrates by weak non-covalent interactions. The amino acids Gly216 forms H-bond with carbonyl group while Gln 192 has an H-bond with methoxy group. Glu97 having an H-bond with CH2 and electrostatic interactions are detailed in Fig. 9. The docked ligand forms a stable complex with Factor Xa receptor as depicted in Fig. 10 and the binding free energy value is −5.7 kcal/mol. tabulated in Table 8. The docked ligand embedded in the catalytic site of factor Xa (fXa) as shown in Fig. 11. These preliminary results suggest that the compound having inhibitory activity against the coagulation cascade. Thus the title compound can be developed as drug used for the treatment of Cardiovascular and Cerebrovascular diseases.

5. Conclusions

In the present study, the molecular structure and vibrational frequencies of 1,7,8,9 - tetrachloro-10,10-dimethoxy-4-[3-(4-benzylpiperazine-1-yl) propyl]-4-azatricyclo [5.2.1.$0^{2,6}$] dec-8-ene-3,5-dione have been studied theoretically and experimentally. The calculated geometrical parameters of the title compound are in good agreement with experimental values. The small difference between experimental and calculated vibrational wavenumbers was that, the experimental results belong to solid phase and the theoretical calculations belong to gaseous phase. For the title compound HOMO is delocalized over cyclohexene ring and LUMO is delocalized at phenyl ring. HOMO-LUMO band gap of the title compound is found to be 3.144 eV and shows the stability of the molecule. From NBO analysis strong interactions are C_{13}-O_{18} from N_{15}, C_{16}-O_{17} from N_{15}, N_{15}-$C_{16}$from O_{17}, C_5-C_{16} from O_{17}, C_{13}-$N_{15}$from O_{18} and C_4-C_{13} from O_{18}. The MEP studies shows that the title compound and halogen substitution the electrophilic region is strongly over N_{38} of piperazine ring and nucleophilic region is maximum pronounced over the methoxy group. The compound is optically active because the calculated first hyperpolarizability of the compound is comparable with the standard compound. By DFT calculations we were able to calculate the ALIE values, beside benzene ring, hydrogen atoms are prone to electrophilic attacks. Thanks to the mapping of the Fukui function values to the electron density surface we have also determined that carbon atom C_{28}, C_{31} and oxygen atoms O_{18}, O_{17} are important reactive centres. The RDF peaks conclude that the compound is stable near moisture. The MD calculations of solubility parameter suggests that it is reasonable to consider PVP as an excipient for TCDBPAD molecule. The title compound can be developed as drug used for the treatment of Cardiovascular and Cerebrovascular diseases.

Acknowledgement

The authors would like to extend their sincere gratitude to Dr. Parameswaran Pattiyil, Department of chemistry, National Institute of Technology Calicut. Thanks to Department of physics, University of Novi Sad for the MD simulations. Part of this work has been performed, thanks for the support received from Schrodinger Inc.

References

[1] L. H. Atherden, Bentley and Driver's Text Book of Pharmaceutical Chemistry, eighth ed., Oxford Medicinal Publication, (2004) 372-377, 204-205.

[2] A. H. Beckett, J. B. Stenlake, Practical Pharmaceutical Chemistry, Fourth ed., CBS Publishers and Distributors, (2003).

[3] C. C. J. Carpenter, M. A. Fischl, S. M. Hammer, M. S. Hirsch, D. M. Jacobsen, D. A. Katzenstein, J. S. G. Montaner, D. D. Richman, M. S. Saag, R. T. Schooley, M. A. Thompson, S. Vella, P. G. Yeni, P. A. Volberding, Antiretroviral Therapy for HIV infection in 1998 updated recommendations of the international AIDS society-USA panel, J. Am. Med. Assoc. 280 (1998) 78-86.

[4] M. Bartok, K. Felfoldi, E. Karpati, A. Molnar, L. Szporny, 3-[4-(2'-Pyridyl)-piperazin-1-yl]-1-(3,4,5-trimethoxybenzoyloxy)-propane or a pharmaceutically acceptable acid-addition salt thereof in a composition with anti-arrhythmic activity. U.S. Pat. US4196206, (1980).

[5] R. Mlynárová, D. Tazká, E. Racanská, J. Kyselovic, P. Svec, Effects of a fluorophenyl) piperazine deriv0ative (substance IIIv) on cardiovascular function. Ceska Slov. Farm. 49 (2000) 177-180.

[6] R. Filosa, A. Peduto, P. de Caprariis, C. Saturnino, M. Festa, A. Petrella, A. Pau, G. A. Pinna, P. La Colla, B. Busonera, R. Loddo, Synthesis and antiproliferative properties of N3/8-disubstituted 3,8-diazabicyclo[3.2.1]octane analogues of 3,8-bis[2-(3,4,5-trimethoxyphenyl)-pyridin-4-yl]methyl-piperazine, Eur. J. Med. Chem. 42 (2007) 293-306.

[7] Y. J. Shaw, Y. T. Yang, J. B. Garrison, N. Kyprianou, C. S. Chen, Pharmacological exploitation of the alpha1-adrenoreceptor antagonist doxazosin to develop a novel class of antitumor agents that block intracellular protein kinase B/Akt activation, J. Med. Chem. 47 (2004) 4453-4462.

[8] S. Richter, C. Parolin, M. Palumbo, G. Palu, Antiviral properties of quinolone-based drugs. Curr. Drug. Targets Infect. Disord. 4 (2004) 111-116.

[9] T. M. Chan, K. Cox, W. Feng, M. W. Miller, D. Weston, S. W. McCombie, Piperidinyl piperazine derivatives useful as inhibitors of chemokine receptors. U.S. Pat. 2006223821, (2006).

[10] M. Kimura, T. Masuda, K. Yamada, N. Kawakatsu, N. Kubota, M. Mitani, K. Kishii, M. Inazu, Y. Kiuchi, K. Oguchi, T. Namiki, Antioxidative activities of novel diphenylalkyl piperazine derivatives with high affinities for the dopamine transporter, Bioorg. Med. Chem. Lett. 14 (2004) 4287-4290.

[11] A. Foroumadi, S. Emami, A. Hassanzadeh, M. Rajaee, K. Sokhanvar, M. H. Moshafi, A. Shafiee, Synthesis and antibacterial activity of N-(5-benzylthio-1,3,4-thiadiazol-2-yl) and N-(5-benzylsulfonyl-1,3,4-thiadiazol-2-yl) piperazinyl quinolone derivatives. Bioorg. Med. Chem. Lett. 15 (2005) 4488-4492.

[12] A. K. Dutta, S. K. Venkataraman, X. S. Fei, R. Kolhatkar, S. Zhang, M. E. Reith, Synthesis and biological characterization of novel hybrid 7-[[2-(4-phenyl-piperazin-1-yl)-ethyl]-propyl-amino]-5,6,7,8-tetrahydro-naphthalen-2-ol and their heterocyclic bioisosteric analogues for dopamine D2 and D3 receptors, Bioorg. Med. Chem. 12 (2004) 4361-4373.

[13] V. Cecchetti, F. Schiaffella, O. Tabarrini, A. Fravolini, (1,4-Benzothiazinyloxy) alkylpiperazine derivatives as potential antihypertensive agents, Bioorg. Med. Chem. Lett. 10 (2000) 465-468.

[14] L. Betti, M. Zanelli, G. Giannaccini, F. Manetti, S. Schenone, G. Strappaghetti, Synthesis of new piperazine-pyridazinone derivatives and their binding affinity toward alpha1-, alpha2-adrenergic and 5-HT1A serotoninergic receptors. Bioorg. Med. Chem. 14 (2006) 2828-2836.

[15] J. Obniska, M. Kołaczkowski, A. J. Bojarski, B. Duszyńska, Synthesis, anticonvulsant activity and 5-HT_{1A}, 5-HT_{2A} receptor affinity of new N-[(4-arylpiperazin-1-yl)-alkyl] derivatives of 2-azaspiro[4.4]nonane and [4.5]decane-1,3-dione,. Eur. J. Med. Chem. 41 (2006) 874-881.

[16] J. Kossakowski, M. Pakosinska-Parys, M. Struga, I. Dybala, A. E. Koziol, P. La Colla, L. E. Marongiu, C. Ibba, D. Collu, R. Loddo, Synthesis and Evaluation of in Vitro Biological Activity of 4-Substituted Arylpiperazine Derivatives of 1,7,8,9-Tetrachloro-

10,10-dimethoxy-4-azatricyclo[5.2.1.$0^{2,6}$]dec-8-ene-3,5-dione, Molecules 14 (2009) 5189-5202.

[17] M. Rani, P. Parthiban, R. Ramachandran, S. Kabilan, Design and synthesis of novel piperazine unit condensed 2, 6-diarylpiperidin-4-one derivatives as antituberculosis and antimicrobial agents, Med. Chem. Res. 21 (2012) 653-662.

[18] S. Armakovic, S. J. Armakovic, J. P. Setrajcic, I. J. Serajcic, Active components of frequently used β- blockers from the aspect of computational study. J. Mol. Model 18 (2012) 4491-4501.

[19] C. A. Peri, New polychlorinated derivatives containing the ring of 1,4-endomethylenecyclohexane, Gazz. Chim. Ital. 85 (1955) 1118-1140.

[20] M. J. Frisch, G. W. Trucks, H. B. Schlegel, G. E. Scuseria, M. A. Robb, J. R. Cheeseman, G. Scalmani, V. Barone, B. Mennucci, G. A. Petersson, H. Nakatsuji, M. Caricato, X. Li, H. P. Hratchian, A. F. Izmaylov, J. Bloino, G. Zheng, J. L. Sonnenberg, M. Hada, M. Ehara, K. Toyota, R. Fukuda, J. Hasegawa, M. Ishida, T. Nakajima, Y. Honda, O. Kitao, H. Nakai, T. Vreven, J. A. Montgomery Jr., J. E. Peralta, F. Ogliaro, M. Bearpark, J. J. Heyd, E. Brothers, K. N. Kudin, V. N. Staroverov, T. Keith, R. Kobayashi, J. Normand, K. Raghavachari, A. Rendell, J. C. Burant, S. S. Iyengar, J. Tomasi, M. Cossi, N. Rega, J. M. Millam, M. Klene, J. E. Knox, J. B. Cross, V. Bakken, C. Adamo, J. Jaramillo, R. Gomperts, R. E. Stratmann, O. Yazyev, A. J. Austin, R. Cammi, C. Pomelli, J. W. Ochterski, R. L. Martin, K. Morokuma, V. G. Zakrzewski, G. A. Voth, P. Salvador, J. J. Dannenberg, S. Dapprich, A. D. Daniels, O. Farkas, J. B. Foresman, J. V. Ortiz, J. Cioslowski, D. J. Fox, Gaussian 09, Revision B.01, Gaussian Inc, Wallingford CT, 2010.

[21] J. B. Foresman, in: E. Frisch (Ed.), Exploring Chemistry with Electronic Structure Methods: A Guide to Using Gaussian, Gaussian Inc., Pittsburg, PA, 1996.

[22] J. M. L. Martin, C. V. Alsenoy, GAR2PED, A Program to Obtain a Potential Energy Distribution from a Gaussian Archive Record, University of Antwerp, Belgium, 2007.

[23] R. Dennington, T. Keith, J. Millam, GaussView, Version 5, Semichem Inc., Shawnee Mission KS, 2009.

[24] A. D. Becke, Density-functional thermochemistry. III. The role of exact exchange, J. Chem. Phys. 98(7) (1993) 5648-5652.

[25] J. L. Banks, H. S. Beard, Y. Cao, A. E. Cho, W. Damm, R. Farid, A. K. Felts, T. A. Halgren, D. T. Mainz, J. R. Maple, Integrated modeling program, applied chemical theory (IMPACT), J. Comput. Chem. 26(16) (2005) 1752-1780.

[26] H. J. Berendsen, J. P. Postma, W. F. van Gunsteren, J. Hermans, Interaction models for water in relation to protein hydration, in Intermolecular forces. 1981, Springer. p. 331-342.

[27] N. R. Conley, R. J. Hung, C. G. Willson, , A New Synthetic Route to Authentic N-Substituted Aminomaleimides, J. Org. Chem. 70 (2005) 4553-4555.

[28] T. M. V. D. Pinho e Melo, A. M. T. D. P. Cabral, A. M. R. Gonsalves, A. M. Beja, J. A. Paixao, M. R. Silva, L. A. daVeiga, A New Route to Cross-Conjugated Bis(enamines) and an Unusual Reaction with DDQ, J. Org. Chem. 64 (1999) 7229-7232.

[29] D. Lee, T. M. Swager, Toward Isolated Molecular Wires: A pH-Responsive Canopied Polypyrrole, Chem. Mater. 17 (2005) 4622-4629.

[30] B. Bartkowska, F. M. Bohnen, C. Kruger, W. F. Maier, 4-(1,7,8,9,10,10-Hexachloro-3,5-dioxo-4-aza- tricyclo[5.2.1.0 ^{2,6}]dec-8-en-4-yl) butyric Acid Toluene Solvate, Acta Cryst. C53 (1997) 521-522.

[31] I. N. Tarabara, Y. S. Bondarenko, A. A. Zhurakovskii, L. I. Kas'yan, New derivatives of 2-(3,5-Dioxo-4-azatricyclo [5.2.1.0^{2,6}-endo] dec-8-en-4-yl) acetic acid. Synthesis and reactivity, Russ. J. Org. Chem. 43 (2007) 1297-1304

[32] H. B. Burgi, J. D. Dunitz, Structure Correlation, vol. 2, VCH, Weinheim (1994) 741-784.

[33] R. Manohar, M. Harikrishna, C. R. Ramanathan, M. SureshKumar, K. Gunasekaran, 1,7,8,9,10,10-Hexachloro-4-(thiophen-2-ylmethyl)-4-azatricyclo[5.2.1.0^{2,6}]dec-8-ene-3,5-dione, Acta Crystallogr. E67 (2011) 2391-2398.

[34] L. I. Kasyan, V. A. Palchikov, A. V. Turov, S. A. Pridma, A. V. Tokar, Cage-like amines in the synthesis and oxidation of camphor-10-sulfonic acid amides, Russ. J. Org. Chem. 45 (2009) 1007-1017.

[35] L. I. Kasyan, S. V. Sereda, K. A. Poteknin, A. O. Kasyan, Azabrendanes. I. Synthesis, structure and spectral parameters of N-(arylsulfonyl)-exo-2-hydroxy-4-azatricyclo[4.2.1.0^{3,7}] nonanes, Heteroatom Chem. 8 (1997) 177-184.

[36] A. A. El-Emam, A. M. S. Al-Tamimi, K. A. Al-Rashood, H. N. Misra, V. Narayan, O. Prasad, L. Sinha, Structural and spectroscopic characterization of a novel potential chemotherapeutic agent 3-(1-adamantyl)-1-{[4-(2-methoxyphenyl) piperazin-1-yl] methyl}-4-methyl-1H-1, 2, 4-triazole-5(4H)-thione by first principle calculations, J. Mol. Struct. 1022 (2012) 49-60.

[37] Y. H. Gao, X. J. Liu, L. Sun , W. J. Le, Bis (piperazine-1,4-diium) hexachloridobismuthate (III) chloride monohydrate, Acta Cryst. E67 (2011) 1688-1688.

[38] N. P. G. Roeges, A Guide to the Complete Interpretation of the Infrared Spectra of Organic Structures Wiley, New York, (1994).

[39] N. B. Colthup, L.H. Daly S.E. Wiberly, Introduction to Infrared and Raman Spectroscopy Academic Press, New York, (1990).

[40] R. Renjith, Y. S. Mary, C. Y. Panicker, H. T. Varghese, M. P. Parys, C. V. Alsenoy, T. K. Manojkumar, Spectroscopic (FT-IR, FT-Raman), first order hyperpolarizability, NBO analysis, HOMO and LUMO analysis of 1,7,8,9-tetrachloro-10,10-dimethoxy-4-[3-(4-phenylpiperazin-1-yl)propyl]-4-azatricyclo[5.2.1.$0^{2,6}$]dec-8-ene-3,5-dione by density functional methods, Spectrochim. Acta 124 (2014) 500-513.

[41] I. C. H. Castaneda, J. L. Jios, O. E. Piro, G. E. Tobon, C. O. D. Vedova, Conformational and vibrational analysis of S-(2-methoxyphenyl)-4substituted-benzenecarbothioates, using X-ray, infrared and Raman spectroscopy and theoretical calculations, J. Mol. Struct. 842 (2007) 46-54.

[42] R. Zhang, X. Li, X. Zhang, Molecular structure and vibrational spectra of phenobaraitone by density functional theory and ab initio Hartree Fock calculations, Front. Chem. China 6 (2011) 358-366.

[43] G. Socrates, Infrared Characteristic Group Frequencies John Wiley and Sons, New York, (1981).

[44] K. Nakanishi, Infrared Absorption Spectroscopy Practical Holden Day, San Francisco, (1962).

[45] S. Kundoo, A. N. Banerjee, P. Saha, K. K. Chattophyay, Synthesis of crystalline carbon nitride thin films by electrolysis of methanol-urea solution, Mater. Lett. 57 (2003) 2193-2197.

[46] M. Silverstein, G. C. Basseler, C. Morill, Spectrometric Identification of Organic Compounds, John Wiley and Sons Inc. Singapore (1991).

[47] L. I. Kasyan, A. V. Serbin, A. O. Kasyan, D. V. Karpenko, E. A. Golodaeva, Reactions of Bi-, Tri-, and tetracyclic amines with succinic anhydride, Russ. J. Org. Chem. 44 (2008) 340-347.

[48] L. H. Daly, S. E. Wiberly, Introduction to Infrared and Raman Spectroscopy Ed. 3, academic Press, Boston (1990).

[49] K. Felfoldi, M. Sutyinszky, N. Nagy, I. Palinko, Synthesis of E- and Z-o-methoxy-substituted 2, 3-diphenylpropenoic acids and its methyl esters, Synth. Commun. 30 (2000) 1543-1553.

[50] C. Lee, W. Yang, R. G. Parr, Development of the Colle-Salvetti correlation-energy formula into a functional of the electron density Phys. Rev. 37B (1998) 785-789.

[51] E. F. Mooney, The infra-red spectra of chloro-and bromobenzene derivatives-II. nitrobenzenes, Spectrochim. Acta 20 (1964) 1021-1032.

[52] E. F. Mooney, The infrared spectra of chloro- and bromobenzene derivatives-I: Anisoles and phenetoles, Spectrochim. Acta 19 (1963) 877-887.

[53] N. Sundaraganesan, C. Meganathan, B. D. Joshua, P. Mani, A. Jayaprakash, Molecular structure and vibrational spectra of 3chloro-4-fluorobenzonitrile by ab initio HF and density functional method, Spectrochim. Acta 71A (2008) 1134-1139.

[54] G. Varsanyi, Assignments of Vibrational Spectra of Seven Hundred Benzene Derivatives, Wiley: New York, (1974).

[55] P. Pazdera, H. Divisova, H. Havilsova, P. Borek, Synthesis of N-(2 Cyanophenyl) chloromethanimidoyl Chloride, Molecules 5 (2000) 189-194.

[56] H. T. Varghese, C. Y. Panicker, D. Philip, P. Pazdera, Vibrational spectroscopic studies and ab initio calculations of 2-cyanophenyl isocyanid dichloride, Spectrochim. Acta 67A (2007) 1055-1059.

[57] H. Arslan, U. Florke, N. Kulcu, G. Binzet, The molecular structure and vibrational spectra of 2-chloro-N-(diethylcarbamothioyl)benzamide by Hartree-Fock and density functional methods, Spectrochim. Acta 68A (2007) 1347-1355.

[58] H. L. Spell, Determination of piperazine rings in ethyleneamines, poly (ethyleneamine), and polyethylenimine by infrared spectrometry, Anal. Chem. 41 (1969) 902-905.

[59] A. S. El-Azab, Y. S. Mary, C. Y. Panicker, A. A.-M A-Aziz, A. Magda, El-Sherbeny, C. V. Alsenoy, DFT and experimental (FT-IR and FT-Raman) investigation of vibrational spectroscopy and molecular docking studies of 2-(4-oxo-3-phenyl-3,4-dihydroquinazolin-2-ylthio)-N-(3,4,5 trimethoxyphenyl) acetamide, J. Mol. Struct. 1113 (2016) 133-145.

[60] F. J. Luque, J. M. Lopez, M. Orozco, Perspective on electrostatic interactions of a solute with a continuum, a direct utilization of ab initio molecular potentials for the prevision of solvent effects, Theor. Chem. Acc. 103 (2000) 343-345.

[61] P. Politzer, J. S. Murray, in: D. L. Beveridge, R. Lavery, (Eds.), Theoretical Biochemistry and Molecular Biophysics, A Comprehensive Survey, Protein, Vol. 2, Adenine Press, Schenectady, New York, 1991.

[62] E. D. Glendening, A. E. Reed, J. E. Carpenter, F. Weinhold, NBO Version 3.1, Gaussian Inc., Pittsburgh, PA, 2003.

[63] M. Adant, M. Dupuis, J. L. Bredas, Ab initio study of the nonlinear optical properties of urea: Electron correlation and dispersion effects, Int. J. Quantum. Chem. 56 (1995) 497-507.

[64] R. Renjith, Y. Sheena Mary, C. Yohannan Panicker, Hema Tresa Varghese, Magdalena Pakosinska-Parys, C. Van Alsenoy, T. K. Manojkumar, Vibrational spectroscopic and computational study of 1,7,8,9-Tetrachloro-4-(4-bromo-butyl)-10,10-dimethoxy-4-aza-tricyclo[5.2.1.$0^{2,6}$] dec-8-ene-3,5-dione, Spectrochim. Acta Part A 124 (2014) 480-491.

[65] J.S. Murray, J.M. Seminario, P. Politzer, P. Sjoberg, Average local ionization energies computed on the surfaces of some strained molecules, Int. J. Quantum Chem. 38 (S24) (1990) 645-653.

[66] P. Politzer, F. Abu-Awwad, J.S. Murray, Comparison of density functional and Hartree–Fock average local ionization energies on molecular surfaces, Int. J. Quantum Chem. 69(4) (1998) 607-613.

[67] A. Toro-Labb_e, P. Jaque, J.S. Murray, P. Politzer, Connection between the average local ionization energy and the Fukui function, Chem. Phys. Lett. 407(2005) 143-146.

[68] R. G. Parr, Density Functional Theory of Atoms and Molecules, in Horizons of Quantum Chemistry, Springer, (1980) 5-15.

[69] A. Michalak, F. De Proft, P. Geerlings, R. Nalewajski, Fukui functions from the relaxed Kohn-Sham orbitals, J. Phys. Chem. A 103 (1999) 762-771.

[70] R. V. Vaz, J. R. Gomes, C. M. Silva, Molecular dynamics simulation of diffusion coefficients and structural properties of ketones in supercritical CO 2 at infinite dilution, J. Supercritic. Fluids, 107 (2016) 630-638.

[71] D. J. Greenhalgh, A. C. Williams, P. Timmins, P. York, Solubility parameters as predictors of miscibility in solid dispersions, J. Pharm. Sci. 88 (1999) 1182–1190.

[72] R. C. Rowe, Adhesion of film coatings to tablet surfaces—a theoretical approach based on solubility parameters, Int. J. Pharm. 41 (1988) 219-222.

[73] R. C. Rowe, Interactions in coloured powders and tablet formulations: a theoretical approach based on solubility parameters, Int. J. Pharm. 53 (1989) 47-51.

[74] Y. K. Lee, M. R. Player, Developments in Factor Xa Inhibitors for the Treatment of Thromboembolic Disorders, Med. Res. Rev. 31 (2011) 202-283.

[75] E. M. Antman, Hirudin in Acute Myocardial Infarction. Safety Report from the Thrombolysis and Thrombin Inhibition in Myocardial Infarction (TIMI) 9A Trial, Circulation 90 (1994) 1624-1630.

[76] Randomized Trial of Intravenous Heparin Versus Recombinant Hirudin for Acute Coronary Syndromes. The Global Use of Strategies to Open Occluded Coronary Arteries GUSTO IIa Investigators, Circulation 90 (1994) 1631-1637.

[77] S. Komoriya, N. Haginoya, S. Kobayashi, T. Nagata, A. Mochizuki, M. Suzuki, T. Yoshino, H. Horino, T. Nagahara, M. Suzuki, Y. Isobe , T. Furugoori, Design, synthesis, and biological activity of non-basic compounds as factor Xa inhibitors: SAR study of S1 and aryl binding sites, Bioorg. Med. Chem. 13 (2005) 3927-3954.

[78] K. Padmanabhan, K. P. Padmanabhan, C. H. Park, W. Bode, R. Huber. D. T. Blankenship, A. D. Cardin, W. Kisiel, Structure of human Des (1-45) Factor Xa at 2.2A resolution, J. Mol. Biol. 232 (1993) 947-966.

[79] N. Haginoya, S. Kobayashi, S. Komoriya, T. Yoshino, M. Suzuki, T. Shimada, K. Watanabe, Y. Hirokawa, T. Furugori, T. Nagahara, Synthesis and Conformational Analysis of a Non-Amidine Factor Xa Inhibitor That Incorporates 5-Methyl-4,5,6,7-tetrahydrothiazolo [5, 4-c] pyridine as S4 Binding Element, J. Med. Chem. 47 (2004) 5167-5182.

[80] G. M. Morris, R. Huey, W. Lindstrom, M. F. Sanner, R. K. Belew, D. S. Goodsell, A. J. Olson, Auto dock 4 and Auto Dock Tools 4: automated docking with selective receptor flexibility, J. Comput. Chem. 16 (2009) 2785-2791.

[81] O. Trott, A. J. Olson, AutoDock Vina: Improving the speed and accuracy of docking with a new scoring function, efficient optimization and multi-threading, J. Comput. Chem. 31 (2010) 455-461.

[82] G. M. Morris, D. S. Goodsell, R. S. Halliday, R. Huey, W. E. Hart, R. Belew, A. J. Olson, Automated docking using a Lamarckian genetic algorithm and an empirical binding free energy function, J. Comput. Chem. 19 (1998) 1639-1662.

Figure Caption

Fig 1 FT-IR

Fig 2 FT-Raman

Fig 3 Molecule

Fig 4 HOMO-LUMO

Fig 5 MEP

Fig 6 ALIE

Fig 7 Fukui

Fig 8 RDF

Fig 9 Docking

Fig 10 Docking

Fig 11 Docking

Table Caption

Table 1 Geometrical Parameters

Table 2 Frequency

Table 3 HOMO-LUMO

Table 4 NBO-1

Table 5 NBO-2

Table 6 NLO of Substitution

Table 7 Solubility parameter

Table 8 Docking

Graphical Abstract

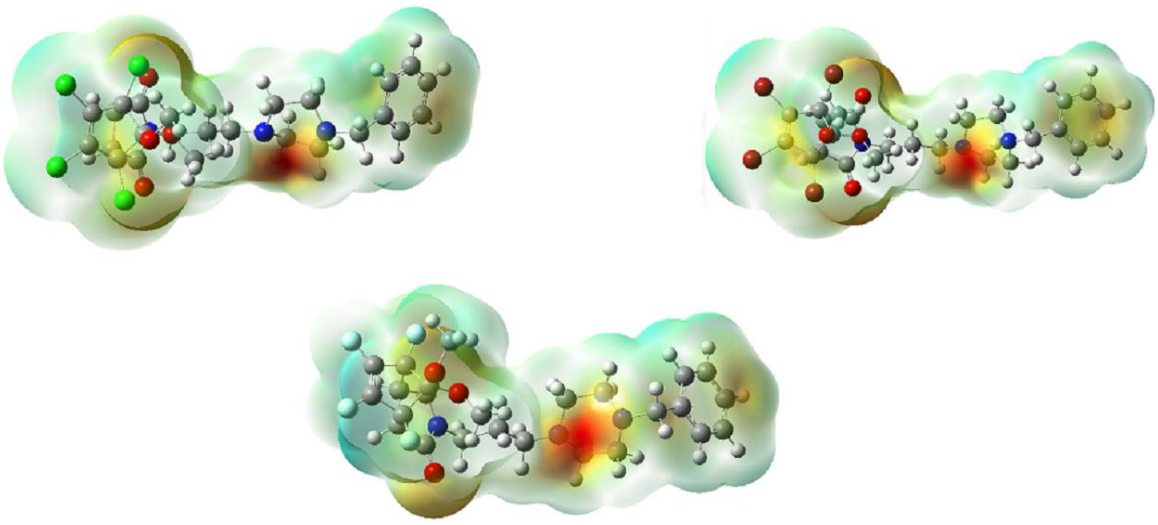

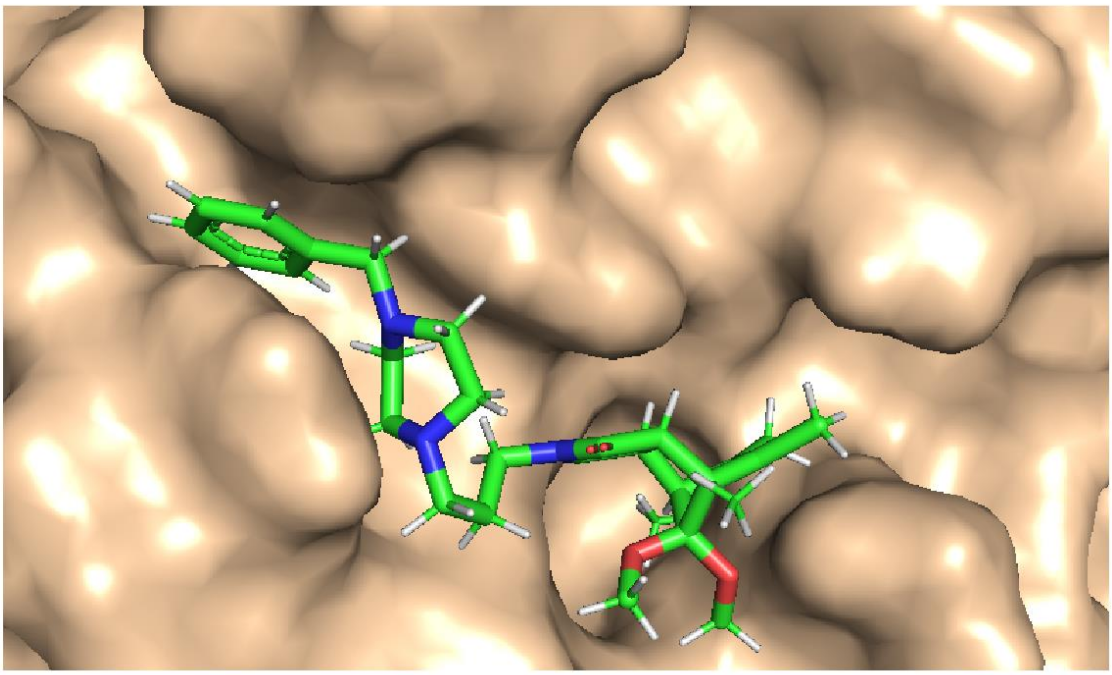

Figures

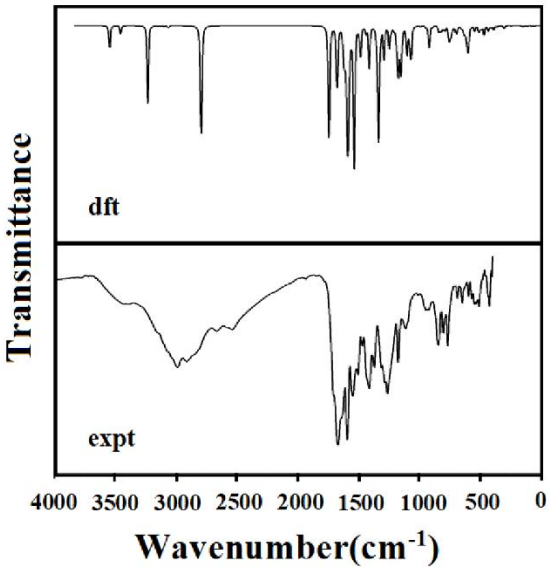

Fig. 1. FT-IR spectrum of TCDBPAD

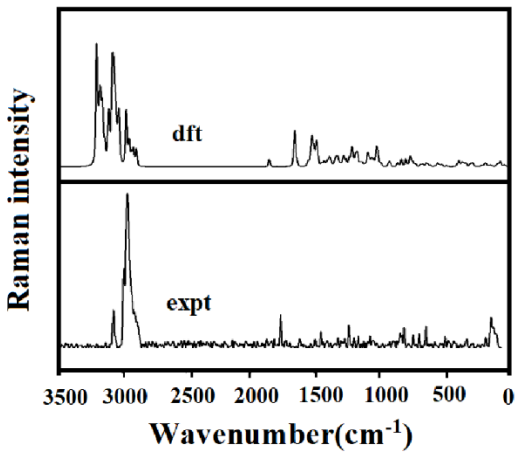

Fig. 2. FT-Raman spectrum of TCDBPAD

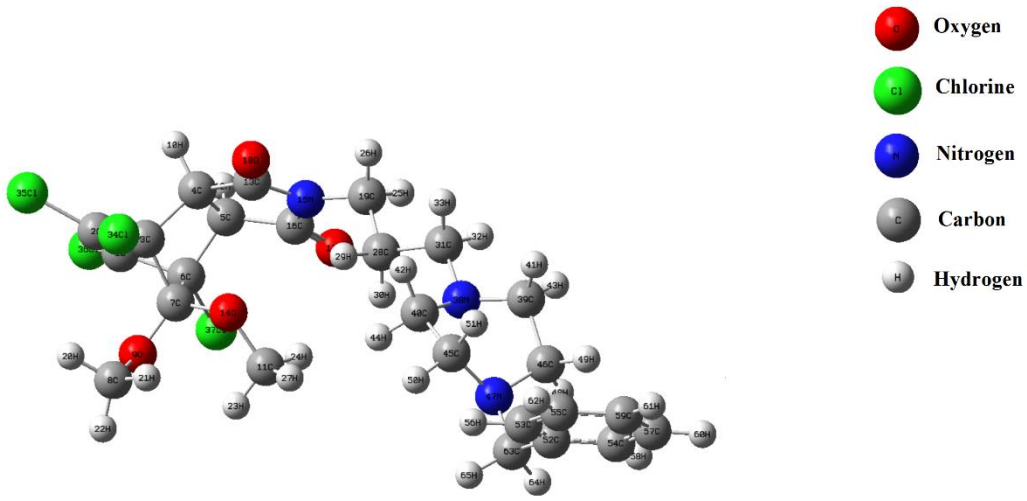

Fig. 3. Optimized geometry of TCDBPAD

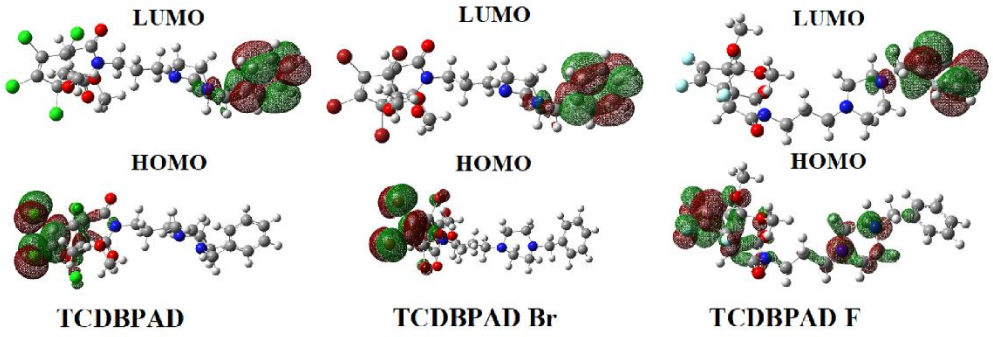

Fig. 4. HOMO-LUMO plots of TCDBPAD with halogen substitutions

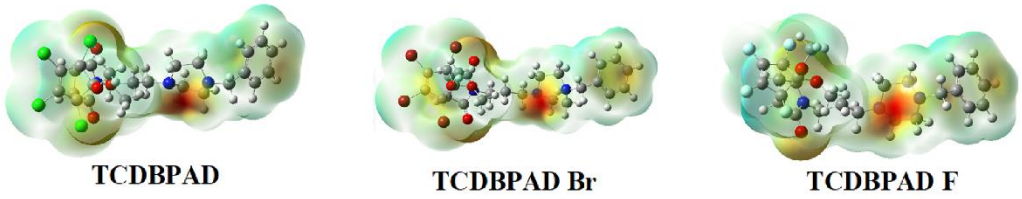

Fig. 5. MEP plots of TCDBPAD with halogen substitutions

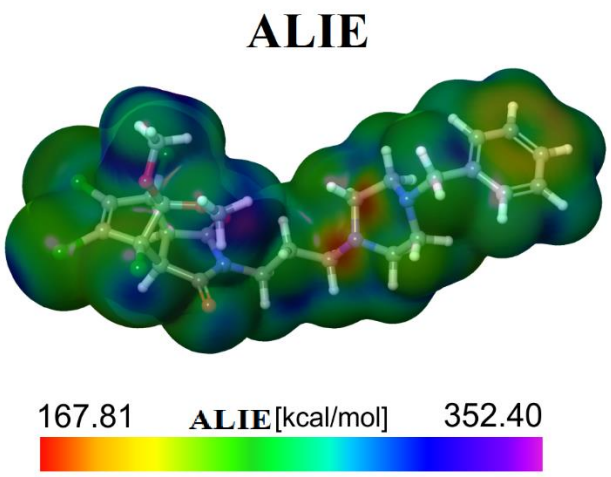

Fig. 6. ALIE surface of TCDBPAD

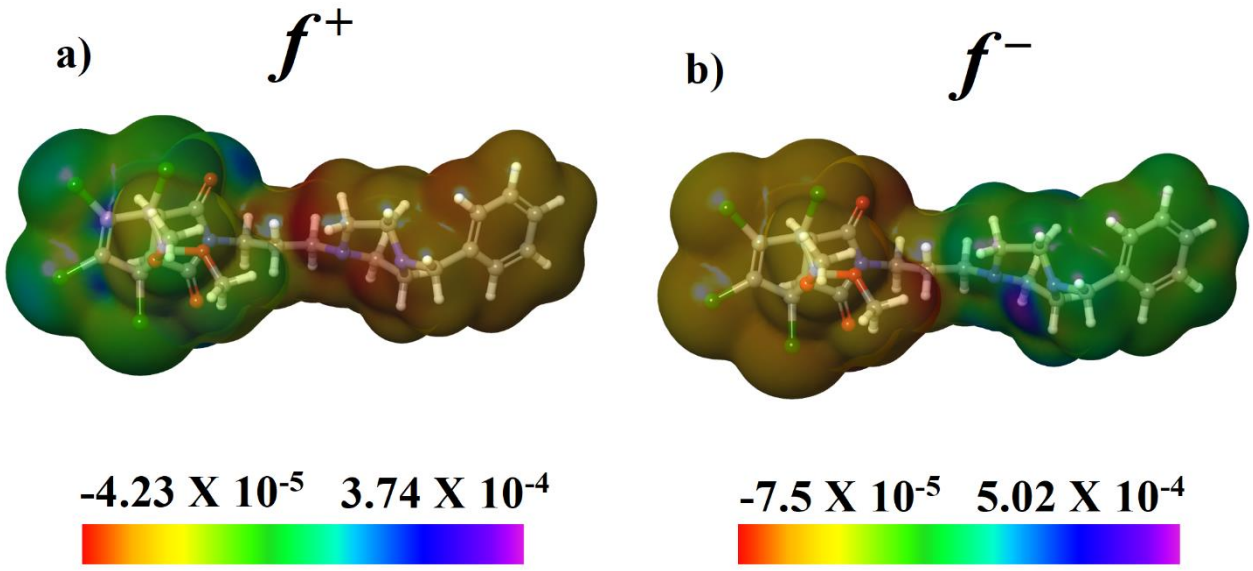

Fig. 7. Fukui functions a) f^+ and b) f^- of TCDBPAD

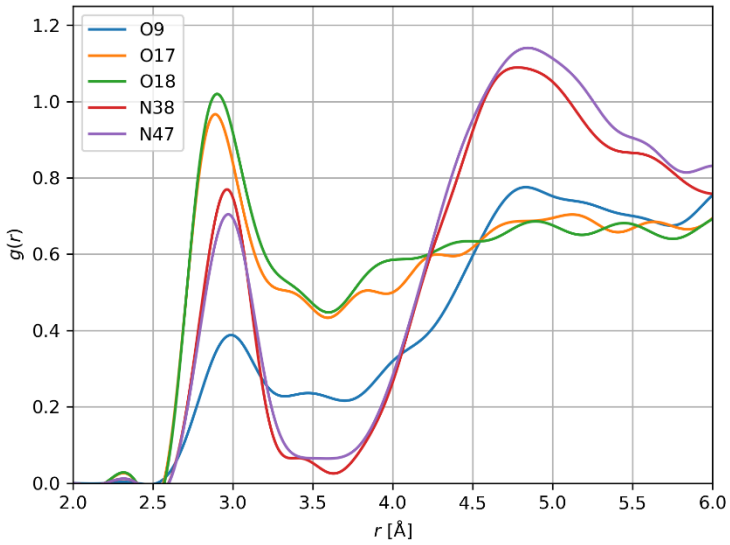

Fig. 8. RDFs of TCDBPAD atoms with significant interactions with water molecules

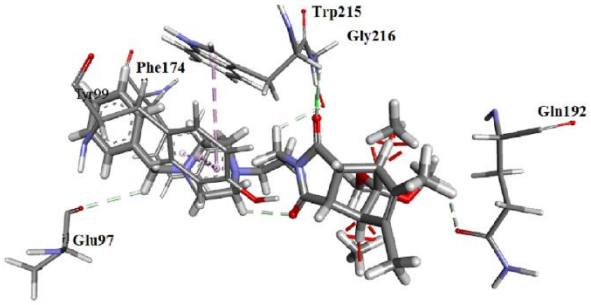

Fig. 9. Ligand interactions TCDBPAD with the amino acids of factor Xa (fXa) inhibitor

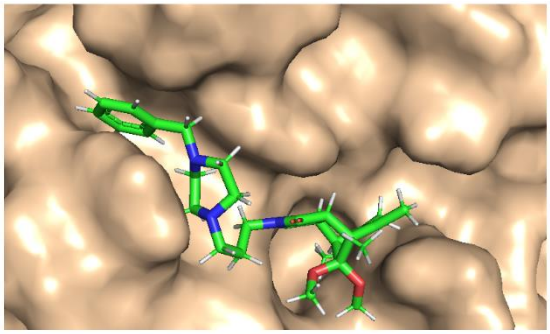

Fig. 10. The docked ligand TCDBPAD at the active site of the receptor

Fig. 11. The docked ligand embedded in the catalytic site of factor Xa (fXa)

Tables

Table 1

Optimized geometrical parameters of TCDBPAD

Bond length (Å)		Bond angle (°)		Dihedral angle (°)	
C_1-C_2	1.3421	C_2-C_1-C_6	107.9	C_6-C_1-C_2-C_3	0.6
C_1-C_6	1.5304	C_2-C_1-Cl_{36}	127.6	C_6-C_1-C_2-Cl_{35}	173.4
C_1-Cl_{36}	1.7185	C_6-C_1-Cl_{36}	124.2	Cl_{36}-C_1-C_2-C_3	−172.9
C_2-C_3	1.5265	C_1-C_2-C_3	107.3	Cl_{36}-C_1-C_2-Cl_{35}	−0.2
C_2-Cl_{35}	1.7193	C_1-C_2-Cl_{35}	127.9	C_2-C_1-C_5-C_5	−70.8
C_3-C_4	1.5711	C_1-C_6-C_5	105.7	C_2-C_1-C_6-C_7	34.9
C_3-C_7	1.5854	C_1-C_6-C_7	99.5	C_2-C_1-C_6-Cl_{37}	160.2
C_3-Cl_{34}	1.7837	C_1-C_6-Cl_{37}	114.6	Cl_{36}-C_1-C_6-C_5	103.0
C_4-C_5	1.5534	C_3-C_2-Cl_{35}	124.4	Cl_{36}-C_1-C_6-C_7	−151.2
C_4-H_{10}	1.0945	C_2-C_3-C_4	104.7	Cl_{36}-C_1-C_6-Cl_{37}	−26.0
C_4-C_{13}	1.5337	C_2-C_3-C_7	99.6	C_1-C_2-C_3-C_4	70.2
C_5-C_6	1.5638	C_2-C_3-Cl_{34}	115.9	C_1-C_2-C_3-C_7	−35.9
C_5-H_{12}	1.0948	C_4-C_3-C_7	102.8	C_1-C_2-C_3-Cl_{34}	−162.9
C_5-C_{16}	1.5373	C_4-C_3-Cl_{34}	114.3	Cl_{35}-C_2-C_3-C_4	−102.9
C_6-C_7	1.5810	C_3-C_4-C_5	103.1	Cl_{35}-C_2-C_3-C_7	151.1
C_6-Cl_{37}	1.7826	C_3-C_4-H_{10}	108.6	Cl_{35}-C_2-C_3-Cl_{34}	24.1

C_7-O_9	1.3823	C_3-C_4-C_{13}	118.8	C_2-C_3-C_4-C_5	−69.3
C_7-O_{14}	1.3903	C_7-C_3-Cl_{34}	117.4	C_2-C_3-C_4-C_{13}	175.2
O_8-C_9	1.4342	C_3-C_7-C_6	91.4	C_7-C_3-C_4-C_5	34.4
C_8-H_{20}	1.0957	C_3-C_7-O_9	118.3	C_7-C_3-C_4-C_{13}	−81.1
C_8-H_{21}	1.0953	C_3-C_7-O_{14}	107.8	Cl_{34}-C_3-C_4-C_5	162.8
C_8-H_{22}	1.0938	C_5-C_4-H_{10}	114.2	Cl_{34}-C_3-C_4-C_{10}	−75.7
C_{11}-O_{14}	1.4421	C_5-C_4-C_{13}	105.0	Cl_{34}-C_3-C_4-C_{13}	47.3
C_{11}-H_{23}	1.0935	C_4-C_5-C_6	103.1	C_2-C_3-C_7-C_6	52.6
C_{11}-H_{24}	1.0949	C_4-C_5-H_{12}	114.1	C_2-C_3-C_7-O_9	−58.6
C_{11}-H_{27}	1.0931	C_4-C_5-C_{16}	104.5	C_2-C_3-C_7-O_{14}	171.0
C_{13}-N_{15}	1.3933	H_{10}-C_4-C_{13}	107.3	C_4-C_3-C_7-C_6	−55.1
C_{13}-O_{18}	1.2077	C_4-C_{13}-N_{15}	107.9	C_4-C_3-C_7-O_9	−166.3
C_{16}-N_{15}	1.3917	C_4-C_{13}-O_{18}	127.4	C_4-C_3-C_7-O_{14}	63.4
C_{19}-N_{15}	1.4617	C_6-C_5-H_{12}	109.4	Cl_{34}-C_3-C_7-C_6	178.5
C_{16}-O_{17}	1.2095	C_6-C_5-C_{16}	118.2	Cl_{34}-C_3-C_7-O_9	67.3
C_{19}-H_{25}	1.0950	C_5-C_6-C_7	102.3	Cl_{34}-C_3-C_7-O_{14}	−63.0
C_{19}-H_{26}	1.0959	C_5-C_6-Cl_{37}	115.9	C_3-C_4-C_5-C_6	2.2
C_{19}-C_{28}	1.5340	H_{12}-C_5-C_{16}	107.6	C_3-C_4-C_5-C_{16}	−122.0
C_{28}-H_{29}	1.0966	C_5-C_{16}-N_{15}	107.9	C_{13}-C_4-C_5-C_6	127.3
C_{28}-H_{30}	1.0969	C_5-C_{16}-O_{17}	127.3	C_{13}-C_4-C_5-C_{16}	3.1
C_{28}-C_{31}	1.5342	C_7-C_6-Cl_{37}	116.6	C_3-C_4-C_{13}-N_{15}	116.2
C_{31}-H_{32}	1.0997	C_6-C_7-O_9	107.9	C_3-C_4-C_{13}-O_{18}	−67.9
C_{31}-H_{33}	1.1126	C_6-C_7-O_{14}	116.5	C_5-C_4-C_{13}-N_{15}	1.7
C_{31}-N_{38}	1.4566	O_9-C_7-O_{14}	113.4	C_5-C_4-C_{13}-O_{18}	177.6
N_{38}-C_{39}	1.4574	C_7-O_9-C_8	118.2	C_4-C_5-C_6-C_1	65.4
C_{40}-N_{38}	1.4714	C_7-O_{14}-C_{11}	117.8	C_4-C_5-C_6-C_7	−38.3
C_{39}-H_{41}	1.1096	O_9-C_8-H_{20}	110.7	C_{16}-C_5-C_6-C_1	−179.9
C_{39}-H_{43}	1.0971	O_9-C_8-H_{21}	111.5	C_{16}-C_5-C_6-C_7	76.3
C_{39}-C_{46}	1.5400	O_9-C_8-H_{22}	105.6	C_{16}-C_5-C_6-Cl_{37}	−51.7
C_{40}-H_{42}	1.1089	H_{20}-C_8-H_{21}	109.4	C_4-C_5-C_{16}-N_{15}	−7.0
C_{40}-H_{44}	1.0979	H_{20}-C_8-H_{22}	109.6	C_4-C_5-C_{16}-O_{17}	176.5
C_{40}-C_{45}	1.5438	H_{21}-C_8-H_{22}	109.9	C_6-C_5-C_{16}-N_{15}	−120.8
C_{45}-N_{47}	1.4540	O_{14}-C_{11}-H_{23}	110.9	C_6-C_5-C_{16}-O_{17}	62.6

C_{45}-H_{50}	1.0977	O_{14}-C_{11}-H_{24}	110.5	C_1-C_6-C_7-C_3	−52.0
C_{45}-H_{51}	1.1073	O_{14}-C_{11}-H_{27}	105.6	C_1-C_6-C_7-O_9	68.4
C_{46}-N_{47}	1.4646	H_{23}-C_{11}-H_{24}	109.7	C_1-C_6-C_7-O_{14}	−162.7
C_{46}-H_{48}	1.1005	H_{23}-C_{11}-H_{27}	110.2	C_5-C_6-C_7-C_3	56.6
C_{46}-H_{49}	1.1055	H_{24}-C_{11}-H_{27}	109.9	C_5-C_6-C_7-O_9	176.9
N_{47}-C_{63}	1.4638	N_{15}-C_{13}-O_{18}	124.6	C_5-C_6-C_7-O_{14}	−54.2
C_{52}-C_{53}	1.4032	C_{13}-N_{15}-C_{16}	114.0	Cl_{37}-C_6-C_7-C_3	−175.8
C_{52}-C_{54}	1.4026	C_{13}-N_{15}-C_{19}	122.4	Cl_{37}-C_6-C_7-O_9	−55.4
C_{52}-C_{63}	1.5255	C_{16}-N_{15}-C_{19}	123.3	Cl_{37}-C_6-C_7-O_{14}	73.4
C_{53}-C_{55}	1.3962	N_{15}-C_{16}-O_{17}	124.7	C_3-C_7-O_9-C_8	−68.2
C_{53}-H_{56}	1.0893	N_{15}-C_{19}-H_{25}	106.7	C_6-C_7-O_9-C_8	−169.9
C_{54}-C_{57}	1.3973	N_{15}-C_{19}-H_{26}	106.7	O_{14}-C_7-O_9-C_8	59.5
C_{54}-H_{58}	1.0895	N_{15}-C_{19}-C_{28}	113.0	C_6-C_7-O_{14}-C_{11}	−76.2
C_{55}-C_{59}	1.3975	H_{25}-C_{19}-H_{26}	108.9	C_9-C_7-O_{14}-C_{11}	49.9
C_{55}-H_{62}	1.0885	H_{25}-C_{19}-C_{28}	110.9	C_4-C_{13}-N_{15}-C_{16}	−6.7
C_{57}-C_{59}	1.3965	H_{26}-C_{19}-C_{28}	110.5	C_4-C_{13}-N_{15}-C_{19}	179.2
C_{57}-H_{60}	1.0884	C_{19}-C_{28}-H_{29}	108.5	O_{18}-C_{13}-N_{15}-C_{16}	177.3
C_{59}-H_{61}	1.0882	C_{19}-C_{28}-H_{30}	109.7	C_{13}-N_{15}-C_{16}-C_5	8.8
C_{63}-H_{64}	1.0998	C_{19}-C_{28}-C_{31}	111.4	C_{13}-N_{15}-C_{16}-O_{17}	−174.6
C_{63}-H_{65}	1.0993	C_{29}-C_{28}-H_{30}	107.8	C_{13}-N_{15}-C_{19}-C_{28}	81.5
		H_{29}-C_{28}-C_{31}	110.6	C_{19}-N_{15}-C_{16}-C_5	−177.1
		H_{30}-C_{28}-C_{31}	108.8	C_{19}-N_{15}-C_{16}-O_{17}	−0.5
		C_{28}-C_{31}-H_{32}	108.8	C_{16}-N_{15}-C_{19}-C_{28}	−92.2
		C_{28}-C_{31}-H_{33}	109.2	N_{15}-C_{19}-C_{28}-C_{31}	−175.9
		H_{28}-C_{31}-H_{38}	112.6	C_{19}-C_{28}-C_{31}-N_{38}	−173.7
		H_{32}-C_{31}-H_{33}	106.6	C_{28}-C_{31}-N_{38}-C_{40}	−65.1
		H_{32}-C_{31}-H_{38}	107.6	C_{31}-N_{38}-C_{39}-C_{46}	−166.1
		H_{33}-C_{31}-H_{38}	111.9	N_{38}-C_{39}-C_{46}-C_{47}	−35.0
		C_{31}-H_{38}-C_{39}	113.3	N_{38}-C_{40}- C_{45}-N_{47}	−34.1
		C_{31}-H_{38}-C_{40}	113.0	C_{40}-C_{45}-N_{47}-C_{46}	65.2
		C_{39}-H_{38}-C_{40}	111.0	C_{39}-N_{38}-C_{40}-C_{45}	−29.0
		N_{38}-C_{39}-H_{41}	112.2	C_{40}-N_{38}-C_{39}-C_{46}	65.5
		N_{38}-C_{39}-H_{43}	108.9	C_{39}-C_{46}-N_{47}-C_{45}	−29.0

		N_{38}-C_{39}-C_{46}	110.2	C_{39}-C_{46}-N_{47}-C_{63}	−164.8
		N_{38}-C_{40}-H_{42}	111.4	C_{40}-C_{45}-N_{47}-C_{63}	−159.9
		N_{38}-C_{40}-H_{44}	108.6	C_{54}-C_{52}-C_{53}-C_{55}	0.7
		N_{38}-C_{40}-C_{45}	111.6	C_{63}-C_{52}-C_{53}-C_{55}	−178.2
		H_{41}-C_{39}-H_{43}	106.3	C_{53}-C_{52}-C_{54}-C_{57}	-0.7
		H_{41}-C_{39}-C_{46}	110.1	C_{63}-C_{52}-C_{54}-C_{57}	178.2
		H_{43}-C_{39}-C_{46}	109.0	C_{52}-C_{54}-C_{57}-C_{59}	0.2
		C_{39}-C_{46}-N_{47}	110.8	C_{53}-C_{55}-C_{59}-C_{57}	−0.3
		C_{39}-C_{46}-H_{48}	110.0	C_{54}-C_{57}-C_{59}-C_{55}	0.3
		C_{39}-C_{46}-H_{49}	107.9		
		H_{42}-C_{40}-H_{44}	107.2		
		H_{42}-C_{40}-C_{45}	108.4		
		H_{44}-C_{40}-C_{45}	109.5		
		C_{40}-C_{45}-N_{47}	109.5		
		C_{40}-C_{45}-H_{50}	108.8		
		C_{40}-C_{45}-H_{51}	110.3		
		N_{47}-C_{45}-H_{50}	108.8		
		N_{47}-C_{45}-H_{51}	113.1		
		C_{45}-N_{47}-C_{46}	112.3		
		C_{45}-N_{47}-C_{63}	116.5		
		H_{50}-C_{45}-H_{51}	106.2		
		N_{47}-C_{46}-H_{48}	108.0		
		N_{47}-C_{46}-H_{49}	112.6		
		N_{46}-C_{47}-C_{63}	114.6		
		H_{48}-C_{46}-H_{49}	107.4		
		N_{47}-C_{63}-C_{52}	116.9		
		N_{47}-C_{63}-H_{64}	107.0		
		N_{47}-C_{63}-H_{65}	107.2		
		C_{53}-C_{52}-C_{54}	118.2		
		C_{53}-C_{52}-C_{63}	120.8		
		C_{52}-C_{53}-C_{55}	121.0		
		C_{52}-C_{53}-H_{56}	119.4		
		C_{54}-C_{52}-C_{63}	121.0		

		C_{52}-C_{54}-C_{57}	121.1		
		C_{52}-C_{54}-H_{58}	119.3		
		C_{52}-C_{63}-H_{64}	109.1		
		C_{52}-C_{63}-H_{65}	109.3		
		C_{55}-C_{53}-H_{56}	119.5		
		C_{53}-C_{55}-C_{59}	120.1		
		C_{53}-C_{55}-H_{62}	119.8		
		C_{57}-C_{54}-H_{58}	119.6		
		C_{54}-C_{57}-C_{59}	120.1		
		C_{54}-C_{57}-H_{60}	119.8		
		C_{59}-C_{55}-H_{62}	120.1		
		C_{55}-C_{59}-C_{57}	119.6		
		C_{55}-C_{59}-H_{61}	120.2		
		C_{59}-C_{57}-H_{60}	120.1		
		C_{57}-C_{59}-H_{61}	120.2		
		C_{64}-H_{63}-H_{65}	106.9		

Table 2
Calculated Scaled wavenumbers, observed IR, Raman bands and vibrational assignments of TCDBPAD

B3LYP/6-31(d')			IR ν(cm^{-1})	Raman ν(cm^{-1})	Assignments
ν(cm^{-1})	IR_I	R_A			
3078	23.96	310.05	-	-	νCHIV(93)
3066	40.52	47.84	3069	3068	νCHIV(99)
3058	8.36	103.41	-	3053	νCHIV(99)
3048	13.01	62.12	-	-	νCH_3(99)
3046	4.39	76.61	-	-	νCHIV(95)
3044	9.20	14.74	-	-	νCHIV(98)
3035	7.15	45.53	-	-	νCH_3(99)

3034	21.89	73.57	-	3030	$\nu CH_3(97)$
3019	19.57	26.71	-	-	$\nu CH_3(99)$
3018	9.03	16.53	-	3016	$\nu CH_2(98)$
2991	7.27	32.67	2989	2988	$\nu CH_2(97)$
2991	2.68	120.67	-	-	νCHI(99)
2983	1.83	36.40	-	-	νCHI(100)
2963	34.25	134.84	-	-	νCH_2III(86)
2962	41.70	12.00	-	2961	$\nu CH_2(91)$
2958	58.22	85.08	-	2959	νCH_2III(82)
2953	11.53	37.31	2954	-	$\nu CH_2(86)$
2952	25.00	116.70	-	-	$\nu CH_3(95)$
2947	6.77	46.87	-	-	$\nu CH_2(85)$
2941	31.86	80.31	-	-	$\nu CH_3(100)$
2935	28.31	54.94	-	-	νCH_2III(87)
2930	16.25	43.30	-	-	$\nu CH_2(88)$
2917	50.99	64.85	-	-	νCH_2III(95)
2910	32.61	86.16	-	-	$\nu CH_2(97)$
2857	75.87	121.35	2878	-	νCH_2III(92)
2837	104.79	73.05	2837	2832	νCH_2III(97)
2817	32.46	28.02	-	2817	νCH_2III(98)
2804	45.84	36.22	-	2805	νCH_2III(93)
2782	56.58	46.66	2781	2792	$\nu CH_2(94)$
1786	36.63	16.33	1766	1788	νC=O(82)
1728	498.50	0.30	1698	1727	νC=O(83)
1598	1.51	36.61	1621	1610	νIV(62), δCHIV(12)
1597	57.17	31.74	-	1595	νC=C(76)
1579	0.87	9.16	-	1573	νIV(70)
1493	3.20	9.83	1513	1497	δCH_2III(61)
1479	6.17	1.46	1477	-	νIV(64), δCHIV(26)
1475	4.49	6.75	-	-	δCH_2III(53), $\delta CH_2(29)$

1474	11.89	10.37	-	-	δCH_3(83)
1473	2.47	7.24	-	1473	δCH_2III(79)
1466	0.84	14.26	-	-	δCH_2III(83)
1465	14.85	2.64	-	-	δCH_3(90)
1464	5.67	14.78	-	-	δCH_2(47), δCH_2III(44)
1459	1.13	13.97	-	-	δCH_3(83)
1453	7.84	1.86	-	1453	δCH_3(67), δCH_2(13)
1450	4.08	18.84	1449	-	δCH_2(70), δCH_3(11)
1437	5.13	0.76	1438	-	νIV(45), δCHIV(43)
1437	1.45	3.58	-	-	δCH_3(46), νIV(25)
1432	10.05	15.88	-	1434	δCH_2(89)
1431	19.96	27.39	-	-	δCH_2(88)
1422	1.98	10.59	-	1418	δCH_3(91)
1396	2.30	3.66	1402	1402	δCH_2III(51), δCH_2(25)
1382	8.86	4.40	-	-	δCH_2III(67)
1378	12.28	1.45	1378	1376	δCH_2(36), δCH_2III(35)
1372	49.41	4.91	-	-	δCH_2III(31), δCH_2(25)
1357	91.58	4.26	-	1357	δCH_2III(30), δCH_2(23)
1348	210.27	6.10	1347	-	νCNII(39), δCH_2(32)
1339	98.34	8.44	-	1340	νCNII(49), δCH_2(39)
1331	38.55	13.16	-	-	δCH_2(68)
1327	24.43	0.65	-	-	δCH_2III(61), δCN(18)
1321	8.24	3.19	-	1321	δCH_2III(30), δCN(20)
1309	0.12	0.70	1307	-	νIV(59), δCHIV(39)
1298	11.36	6.96	-	1297	δCH_2(48), δCH_2III(14)
1287	12.69	10.74	-	-	δCH_2(45), νIV(14)
1280	9.84	5.58	-	1280	δCH_2(48)
1274	4.21	8.35	-	-	δCH_2III(61)
1270	1.08	3.42	1270	-	δCHI(68)
1261	12.84	5.56	-	1265	δCHI(73)

1248	18.75	2.29	1246	1252	δCH_2(37), δCH_2III(29)
1236	17.49	7.87	-	1235	δCH_2(44), δCH_2III(23)
1229	7.58	10.86	1229	-	δCH_2III(48)
1226	1.52	2.95	-	-	δCHI(76)
1212	8.43	9.31	1212	1211	δCH_2III(77)
1192	23.15	2.46	1194	1194	δCHI(34)
1191	99.24	1.95	-	-	δCH_3(52), νCO(23)
1188	62.08	8.23	-	-	νCNIII(25)
1178	3.09	2.48	1178	-	δCH_3(53), υCO(47)
1169	21.40	20.92	-	-	νCC(33), δIV(11)
1167	119.31	6.12	-	-	νCO(31), δCO(19)
1164	3.91	5.74	-	-	δCHIV(54)
1161	9.41	7.51	-	1161	δCHIV(27)
1144	15.50	7.51	1151	-	νCNII(17)
1143	15.92	3.68	-	-	υCO(66)
1140	0.11	4.72	1140	-	δCHIV(78)
1135	63.05	2.47	-	1137	νI(46), δI(15), νCCl(12)
1133	51.01	5.26	-	-	δCH_3(62)
1127	33.47	15.10	1121	1121	νCNII(26), δCH_2(13)
1116	12.55	2.78	-	-	νCNIII(30), νCCIII(12)
1107	34.56	2.59	-	-	νCNII(28), δCH_2(13)
1100	129.37	3.74	1100	1106	νI(24), δCC(20), νCO(16)
1091	87.04	6.05	1087	1088	νCO(37), νI(17)
1073	75.09	2.11	-	1071	δCH_2III(39), νCNIII(20)
1068	15.04	0.66	1065	-	δCHIV(59), νIV(36)
1058	37.80	1.84	-	-	δI(22), νI(20), νCCI(11)
1052	25.18	5.33	-	1054	νI(43), νCCII(18), νCN(14)
1047	5.19	18.85	-	1044	δCH_2III(60)
1035	4.21	5.10	1035	-	νCC(45), δCH_2(20)
1031	7.75	5.57	-	-	νCO(62), δCC(13), νI(11)

1016	2.53	13.45	-	1014	δCHIV(42), νIV(27)
1009	6.17	1.89	1010	-	νCC(41), νI(10)
1005	20.26	4.73	1004	-	νCO(28), νI(12)
989	15.15	3.72	-	997	νCO(46), νCCIII(17)
986	15.20	9.07	987	-	νCCIII(22), νCO(21)
979	1.50	25.76	-	-	νIV(54), δIV(36)
970	19.63	5.12	969	973	νCO(43), νI(35)
967	3.73	1.00	-	-	νI(33)
960	2.75	1.85	-	-	νCCIII(28), δCH_2(20)
954	10.21	1.66	-	-	νCNIII(22), δCH_2III(17)
950	1.12	0.16	-	-	γCHIV(84), τIV(14)
947	25.49	3.53	943	948	νCO(42), νI(21), νCCl(11)
924	0.05	0.14	921	930	γCHIV(92)
895	2.92	1.95	-	-	νCCIII(30), γCHIV(21), δCN(23)
893	2.36	0.61	891	893	γCHIV(64)
890	12.25	4.69	-	-	τI(14), νCCI(10), νI(10)
881	7.68	4.77	872	887	τI(21), νCCI(10)
860	7.48	0.35	-	860	δCH_2III(64)
832	3.22	0.38	845	835	δCH_2(49)
828	0.01	4.64	828	824	γCHIV(100)
819	49.53	1.52	-	-	δI(12)
804	11.98	1.54	-	805	νCNIII(40)
797	3.76	9.48	799	-	δCH_2(42), τIV(11)
788	16.75	0.62	778	785	νCNIII(42)
764	14.63	10.95	-	771	νCNIII(51)
747	36.05	0.87	746	754	δCH_2(35)
731	14.72	19.43	-	735	γCHIV(44), γIV(21)
716	3.70	2.52	-	-	δCH_2(36)
713	4.53	4.70	713	711	γC=O(17), τII(12)
700	18.35	2.22	-	-	νCO(18), νCCl(14)

690	30.46	2.72	684	687	τIV(48), γCHIV(35)
690	6.53	0.83	-	-	τI(13)
657	41.63	1.67	-	668	νCCl(43), δII(35)
646	10.28	3.35	-	648	τIV(24), δIII(19)
632	5.82	3.13	633	634	δCO(24)
610	0.06	4.06	-	616	νCCl(45), δIV(36)
610	8.49	0.27	-	-	δCCl(41)
598	4.30	3.79	602	588	δII(36), νCNII(11)
578	6.39	2.46	-	566	δIV(18), τIV(12), δCH_2(11)
545	0.08	1.38	547	546	γCCl(29), τI(23), δC=O(11)
526	18.93	4.85	527	524	δCH_2(13)
509	4.08	3.02	-	505	δIII(53)
494	0.38	0.61	496	488	νCC(17), γC=O((17)
492	8.67	3.24	483	-	δIV(26), δIII(16)
456	3.19	1.50	461	462	τIV(34), γCC(15)
444	9.01	0.41	-	447	δI(18), τIV(17)
405	8.27	0.50	412	-	δIII(14), τIV(11), δCN(10)
404	0.07	0.04	-	403	τIV(81)
390	8.20	0.26	399	384	δCN(23), δCC(10)
377	7.29	3.95	-	-	δCC(22), δC=O(16)
366	9.96	6.82	-	366	νCCl(20)
351	4.18	0.62	-	-	γCN(33), δIII(15), τIII(13)
346	1.06	1.88	-	348	νCCl(41), δI(22)
340	3.12	4.89	-	-	δCO(32), νCCl(31)
332	6.71	1.94	-	-	δCO(43)
331	5.77	0.58	-	331	γCN(32), τIII(15), δIII(13)
323	2.94	3.12	-	-	δCO(21), γCN(15)
312	8.12	3.49	-	317	δCO(24), γCN(10)
283	2.75	3.46	-	281	δCN(30), δC=O(15)
273	2.75	1.41	-	-	δCN(26)

265	3.51	2.99	-	267	δCC(17), τII(14)
259	2.43	2.03	-	254	τIV(13), τIII(11)
244	2.75	0.57	-	232	δCN(20), δCC(17)
218	3.96	0.58	-	219	τIII(39), γCN(19)
203	2.48	0.46	-	-	τCO(36), τCH_3(15)
197	0.14	0.78	-	196	τCH_3(44), δCCl(14)
187	2.24	0.37	-	-	δCCl(28), τCO(21)
184	0.79	1.13	-	-	τIII(10), τII(10), τCO(10)
172	0.09	2.48	-	171	τIII(16), γCN(21)
168	0.16	0.75	-	-	τIII(36), δCCl(17)
164	0.19	1.62	-	-	δCCl(79)
162	0.28	0.66	-	-	δCCl(35), τCH_3(12)
160	1.02	0.79	-	-	τCO(35), δCCl(22)
149	1.47	0.30	-	150	τCO(44)
146	2.05	1.00	-	-	δCCl(22), δCC(16)
133	0.96	0.94	-	-	τCO(35)
127	1.79	1.22	-	128	δCC(17), τII(12)
123	1.46	0.63	-	-	τII(26), γCN(19), τCO(14)
115	0.44	0.19	-	-	τCH_2(33), τCN(33)
107	1.60	0.47	-	110	τIII(41), τII(24)
94	1.68	0.42	-	89	τCO(21)
84	0.29	0.57	-	83	τI(25), τCH_2(18)
78	0.79	2.63	-	-	τCO(17), τI(14)
72	0.15	1.98	-	-	γCCl(27), τCH_2(11)
59	0.10	3.75	-	65	τII(31), τI(22), τCC(13)
54	0.11	1.32	-	-	τII(20), γCCl(20)
52	0.24	2.99	-	-	τCC(28), τII(18), τI(14)
39	0.11	0.79	-	-	τCH_2(27), τCN(17)
26	0.03	1.55	-	-	τIII(70)
21	0.08	0.94	-	-	τCN(31), τCH_2(16)

11	0.02	0.21	-	-	$\tau CH_2(43)$, $\tau CN(12)$
10	0.01	0.42	-	-	$\tau III(29)$, $\tau CH_2(22)$, $\tau CN(13)$

ν-stretching; δ-in-plane deformation; γ-out-of-plane deformation; τ-torsion

Table 3

Chemical descriptors of TCDBPAD with halogen substitutions

	HOMO	LUMO	$I = -E_{HOMO}$	$A = -E_{LUMO}$	ΔE	$\eta = (I-A)/2$	$\mu = -(I+A)/2$	$\omega = \mu^2/2\eta$
TDBPAD	−8.087	−4.943	8.087	4.943	3.144	1.572	−6.515	13.500
TDBPAD Br	−7.750	−4.945	7.750	4.945	2.805	1.403	−6.347	14.357
TDBPAD F	−8.069	−4.944	8.069	4.944	3.425	1.713	−6.507	12.359

Table 4

NBO results showing the formation of Lewis and non-Lewis orbitals

Bond(A-B)	ED/e[a]	EDA%	EDB%	NBO	s%	p%
σC_1-C_2	1.97824	49.97	50.03	$0.7069(sp^{1.53})C$	39.53	60.47
-	−0.79537	-	-	$+0.7074(sp^{1.52})C$	39.63	60.37
πC_1-C_2	1.93817	49.60	50.40	$0.7043(sp^{99.99})C$	0.78	99.22
-	−0.35716	-	-	$+0.7099(sp^{99.99})C$	0.71	99.29
σC_1-C_6	1.95491	49.52	50.48	$0.7037(sp^{1.85})C$	35.04	64.96
-	−0.68814	-	-	$+0.7105(sp^{2.64})C$	27.45	72.55
σC_1-Cl_{36}	1.98385	45.17	54.83	$0.6721(sp^{3.13})C$	24.18	75.82
-	−0.75533			$+ 0.7405(sp^{4.94})Cl$	16.83	83.17
σC_2-C_3	1.95585	49.62	50.38	$0.7044(sp^{1.85})C$	35.06	64.94
-	−0.68912	-	-	$+0.7098(sp^{2.67})C$	27.27	72.73
σC_1-Cl_{35}	1.98368	45.11	54.89	$0.6716(sp^{3.14})C$	24.15	75.85
-	−0.75561	-	-	$+0.7409(sp^{4.95})Cl$	16.82	83.18
σC_3-C_4	1.95171	50.86	49.14	$0.7132(sp^{2.63})C$	27.54	72.46
-	−0.64730	-	-	$+0.7010(sp^{2.76})C$	26.58	73.42

σC_3-C_7	1.93894	52.00	48.00	0.7211($sp^{2.70}$}C	26.99	73.01
-	−0.64999	-	-	+0.6928($sp^{2.69}$)C	27.12	72.88
σC_3-Cl_{34}	1.97855	44.74	55.26	0.6689($sp^{4.66}$)C	17.66	82.34
-	−0.71092	-	-	+0.7434($sp^{5.15}$)Cl	16.26	83.74
σC_4-C_5	1.94613	49.96	50.94	0.7068($sp^{3.05}$)C	24.68	75.32
-	−0.61944	-	-	+0.7074($sp^{3.06}$)C	24.66	75.34
σC_4-C_{13}	1.96505	52.36	47.64	0.7236($sp^{2.98}$)C	25.15	74.85
-	−0.66159	-	-	+0.6902($sp^{1.78}$)C	35.91	64.09
σC_5-C_6	1.95457	49.37	50.63	0.7026($sp^{2.72}$)C	26.86	73.14
-	−0.64979			+0.7115($sp^{2.64}$)C	27.45	72.55
σC_5-C_{16}	1.96469	52.21	47.79	0.7225($sp^{3.02}$)C	24.90	75.10
-	−0.66084			+0.6913($sp^{1.78}$)C	35.94	64.06
σC_6-C_7	1.93690	51.96	48.04	0.7208($sp^{2.74}$)C	26.77	73.23
-	−0.64931	-	-	+0.6931($sp^{2.73}$)C	26.84	73.16
σC_6-Cl_{37}	1.97833	44.94	55.06	0.6704($sp^{4.62}$)C	17.80	82.20
-	−0.70912	-	-	+0.7420($sp^{5.15}$)Cl	16.25	83.75
σC_7-O_9	1.98700	31.75	68.25	0.5635($sp^{3.30}$)C	23.27	76.73
-	−0.89584	-	-	+0.8261($sp^{2.12}$)O	32.03	67.97
σC_7-O_{14}	1.98639	31.24	68.76	0.5589($sp^{3.45}$)C	22.48	77.52
-	−0.89089	-	-	+0.8292($sp^{2.14}$)O	31.89	68.11
σC_8-O_9	1.98644	30.69	69.31	0.5540($sp^{4.14}$)C	19.58	80.42
-	−0.77372	-	-	+0.8325($sp^{3.97}$)O	24.57	75.43
σC_{11}-O_{14}	1.98578	30.16	69.84	0.5492($sp^{4.24}$)C	19.09	80.91
-	−0.77265	-	-	+0.8357($sp^{3.03}$)O	24.79	75.21
σC_{13}-N_{15}	1.98295	35.62	64.38	0.5968($sp^{2.28}$)C	30.44	69.56
-	−0.82322	-	-	+0.8024($sp^{2.05}$)N	32.82	67.18
σC_{13}-O_{18}	1.99057	33.96	66.04	0.5828($sp^{1.98}$)C	33.54	66.46
-	−1.05921	-	-	+0.8126($sp^{1.66}$)O	37.66	62.34
πC_{13}-O_{18}	1.98302	32.18	67.82	0.5672($sp^{99.99}$)C	0.30	99.70
-	−0.39914	-	-	+0.8236($sp^{99.99}$)O	0.54	99.46
σN_{15}-C_{16}	1.98320	64.28	35.72	0.8018($sp^{2.02}$)N	33.14	66.86
-	−0.82758	-	-	+0.5976($sp^{2.27}$)C	30.59	69.41
σN_{15}-C_{19}	1.98111	64.94	35.06	0.8059($sp^{1.96}$)N	33.83	66.17

-	−0.75184	-	-	+0.5921($sp^{3.59}$)C	21.77	78.23
σC_{16}-O_{17}	1.99064	33.94	66.06	0.5826($sp^{2.00}$)C	33.28	66.72
-	−1.06019	-	-	+0.8128($sp^{1.66}$)O	37.62	62.38
πC_{16}-O_{17}	1.98338	31.96	68.04	0.5653($sp^{99.99}$)C	0.41	99.59
-	−0.40345	-	-	+0.8249($sp^{99.99}$)O	0.63	99.37
σC_{19}-C_{28}	1.97279	51.12	48.88	0.7150($sp^{2.38}$)C	29.59	70.41
-	−0.59967	-	-	+0.6991($sp^{2.81}$)C	26.27	73.73
σC_{28}-C_{31}	1.97392	50.19	49.81	0.7084($sp^{2.64}$)C	27.47	72.53
-	−0.58756	-	-	+0.7058($sp^{2.54}$)C	28.23	71.77
σC_{31}-N_{38}	1.97944	39.01	60.99	0.6246($sp^{3.02}$)C	24.86	75.14
-	−0.68825	-	-	+0.7810($sp^{2.31}$)N	30.20	69.80
σN_{38}-C_{39}	1.98175	61.09	38.91	0.7816($sp^{2.37}$)N	29.69	70.31
-	−0.68402	-	-	+0.6238(sp3.12)C	24.30	75.70
σN_{38}-C_{40}	1.98249	61.20	38.80	0.7823($sp^{2.46)}$N	28.87	71.13
-	−0.67074	-	-	+0.6229($sp^{3.17}$)C	23.96	76.04
σC_{39}-C_{46}	1.97836	50.24	49.76	0.7088($sp^{2.59}$)C	27.87	72.13
-	−0.58690	-	-	+0.7054($sp^{2.57}$)C	27.98	72.02
σC_{40}-C_{45}	1.97839	49.82	50.18	0.7058($sp^{2.54}$)C	28.26	71.74
-	−0.58765	-	-	+0.7084($sp^{2.59}$)C	27.88	72.12
σC_{45}-N_{47}	1.98384	38.98	61.02	0.6244($sp^{3.13}$)C	24.23	75.77
-	−0.68989	-	-	+0.7811($sp^{2.27}$)N	30.59	69.41
σC_{46}-N_{47}	1.98279	38.63	61.37	0.6215($sp^{3.17}$)C	23.98	76.02
-	−0.67605	-	-	+0.7834($sp^{2.35)}$N	29.85	70.15
σN_{47}-C_{63}	1.97644	61.02	38.98	0.7811($sp^{2.28}$)N	30.52	69.48
-	−0.68315	-	-	+0.6244($sp^{3.15}$)C	24.08	75.92
σC_{52}-C_{53}	1.97418	50.03	49.97	0.7073($sp^{1.92}$)C	34.19	65.81
-	−0.67898	-	-	+0.7069($sp^{1.76}$)C	36.20	63.80
σC_{42}-C_{54}	1.97438	50.06	49.94	0.7076($sp^{1.91}$)C	34.34	65.66
-	−0.68015			+0.7067($sp^{1.76}$)C	36.27	63.73
πC_{52}-C_{54}	1.65132	49.48	50.52	0.7034($sp^{99.99}$)C	0.01	99.99
-	−0.24136	-	-	+0.7108($sp^{100.00}$)C	0.00	100.00
σC_{52}-C_{63}	1.97587	50.93	49.07	0.7136($sp^{2.18}$)C	31.46	68.54
-	−0.60545	-	-	+0.7005($sp^{2.36}$)C	29.77	70.23

σC_{53}-C_{55}	1.97948	50.31	49.69	0.7093($sp^{1.83}$)C	35.31	64.69
-	−0.68226	-	-	+0.7049($sp^{1.80}$)C	35.76	64.24
πC_{53}-C_{55}	1.66968	50.31	49.69	0.7093($sp^{1.00}$)C	0.00	100.00
-	−0.24544	-	-	+0.7049($sp^{1.00}$)C	0.00	100.00
σC_{54}-C_{57}	1.97936	50.29	49.71	0.7092($sp^{1.84}$)C	35.22	64.78
-	−0.68122	-	-	+0.7050($sp^{1.80}$)C	35.72	64.28
σC_{55}-C_{59}	1.98096	50.06	49.94	0.7075($sp^{1.83}$)C	35.34	64.66
-	−0.68066	-	-	+0.7067($sp^{1.83}$)C	35.38	64.62
σC_{57}-C_{59}	1.98105	50.06	49.94	0.7075($sp^{1.83}$)C	35.38	64.62
-	−0.68145	-	-	+0.7067($sp^{1.82}$)C	35.42	64.58
πC_{57}-C_{59}	1.66603	49.63	50.37	0.7045($sp^{1.00}$)C	0.00	100.00
-	−0.24475	-	-	+0.7097($sp^{1.00}$)C	0.00	100.00
n_1O_9	1.95633	-	-	$sp^{1.32}$	43.17	56.83
-	−0.55802	-	-	-	-	-
n_2O_9	1.90856	-	-	$sp^{99.99}$	0.24	99.76
-	−0.32359	-	-	-	-	-
n_1O_{14}	1.95235	-	-	$sp^{1.31}$	43.32	56.68
-	−0.56939	-	-	-	-	-
n_2O_{14}	1.90829	-	-	$sp^{1.00}$	0.00	100.00
-	−0.32907	-	-	-	-	-
n_2N_{15}	1.58281	-	-	$sp^{99.99}$	0.20	99.80
-	−0.28576	-	-	-	-	-
n_1O_{17}	1.97276	-	-	$sp^{0.62}$	61.76	38.24
-	−0.69378	-	-	-	-	-
n_2O_{17}	1.86985	-	-	$sp^{99.99}$	0.03	99.97
-	−0.28049	-	-	-	-	-
n_1O_{18}	1.97322	-	-	$sp^{0.62}$	61.81	38.19
-	−0.69164	-	-	-	-	-
n_2O_{18}	1.86933	-	-	$sp^{99.99}$	0.03	99.97
-	−0.27815	-	-	-	-	-
n_1Cl_{34}	1.98558	-	-	$sp^{0.19}$	83.74	16.26
-	−0.96771	-	-	-	-	-
n_2Cl_{34}	1.96397	-	-	$sp^{99.99}$	0.02	99.98

-	−0.32341	-	-	-	-	-
n_3Cl_{34}	1.95935	-	-	$sp^{1.00}$	0.00	100.00
-	−0.32502	-		-	-	-
n_1Cl_{35}	1.98646	-	-	$sp^{0.21}$	82.80	17.20
-	−0.95952		-	-	-	-
n_2Cl_{35}	1.96514	-	-	$sp^{99.99}$	0.38	99.62
-	−0.34298	-	-	-	-	
n_3Cl_{35}	1.91874	-	-	$sp^{1.00}$	0.00	100.00
-	−0.33999	-	-	-	-	-
n_1Cl_{36}	1.98623	-	-	$sp^{0.21}$	82.73	17.27
-	−0.95771	-	-	-	-	-
n_2Cl_{36}	1.96474	-	-	$sp^{99.99}$	0.44	99.56
-	−0.34179	-	-	-	-	-
n_3Cl_{36}	1.91620	-	-	$sp^{1.00}$	0.00	100.00
-	−0.33782	-	-	-	-	-
n_1Cl_{37}	1.98572	-	-	$sp^{0.20}$	83.63	16.37
-	−0.96332	-	-	-	-	-
n_2Cl_{37}	1.96375	-	-	$sp^{99.99}$	0.14	99.86
-	−0.31995	-	-	-	-	-
n_3Cl_{37}	1.95864	-	-	$sp^{1.00}$	0.00	100.00
-	−0.32218	-	-	-	-	-
n_1N_{38}	1.88515	-	-	$sp^{7.90}$	11.24	88.76
-	−0.23865	-	-	-	-	-
n_1N_{47}	1.87222	-	-	$Sp^{10.06}$	9.04	90.96
-	−0.22884	-	-	-	-	-

[a] ED/e in a.u.

Table 5

Second-order perturbation theory analysis of Fock matrix in NBO basis corresponding to the intramolecular bonds of TCDBPAD

Donor(i)	Type	ED/e	Acceptor(j)	Type	ED/e	E(2)[a]	E(j)-E(i)[b]	F(i,j)[c]
C_{52}-C_{54}	π	-	C_{53}-C_{55}	π*	0.32725	20.57	0.28	0.068
C_{52}-C_{54}	π	-	C_{57}-C_{59}	π*	0.33212	22.42	0.28	0.071
C_{53}-C_{55}	π	1.66968	C_{52}-C_{54}	π*	0.34688	21.93	0.29	0.071
C_{53}-C_{55}	π	-	C_{57}-C_{59}	π*	0.33212	20.86	0.28	0.068
C_{57}-C_{59}	π	1.66603	C_{52}-C_{54}	π*	0.34688	20.35	0.29	0.068
C_{57}-C_{59}	π	-	C_{53}-C_{55}	π*	0.32725	21.54	0.28	0.070
LPN_{15}	σ	1.58281	C_{13}-O_{18}	π*	0.23191	50.47	0.26	0.108
LPN_{15}	σ	-	C_{16}-O_{17}	π*	0.24272	51.78	0.26	0.108
LPO_{17}	π	1.86985	C_{5}-C_{16}	σ*	0.07452	20.16	0.59	0.099
LPO_{17}	π	-	N_{15}-C_{16}	σ*	0.08987	25.63	0.63	0.115
LPO_{18}	π	1.86933	C_{4}-C_{13}	σ*	0.07415	20.01	0.60	0.099
LPO_{18}	π	-	C_{13}-N_{15}	σ*	0.09077	25.99	0.63	0.115
$LPCl_{35}$	n	-	C_{2}-C_{3}	σ*	0.05851	14.68	0.33	0.064
$LPCl_{36}$	n	1.91620	C_{1}-C_{2}	π*	0.19750	14.97	0.33	0.064

a E(2) means energy of hyperconjugative interactions (stabilization energy).

b Energy difference between donor and acceptor i and j NBO orbitals.

c F(i,j) is the Fock matrix element between i and j NBO orbitals

Table 6

Polarizability values of TCDBPAD and halogen substitutions

	μ	$\alpha \times 10^{-23}$esu	$\beta \times 10^{-30}$esu	$\gamma \times 10^{-37}$esu	MR = 1.333παN = 25.21 α
TCDBPAD	−6.515	4.7836	1.6690	−73.528	120.595
TCDBPAD Br	−6.347	5.1027	1.7503	−82.795	128.639
TCDBPAD F	−6.507	4.1196	2.4111	−61.574	103.855

Table 7

Values of solubility parameters δ [$MPa^{1/2}$] for studied molecules and the excipients

Molecules	δ [$MPa^{1/2}$]
TCDBPAD	19.104
PVP	18.515
Maltose	28.564
Sorbitol	32.425

Table 8

The binding affinity values of different poses of the compound TCDBPAD predicted by Autodock Vina.

Mode	Affinity (kcal/mol)	Distance from best mode (Å)	
–	–	RMSD l.b.	RMSD u.b.
1	−5.7	0.000	0.000
2	−5.6	4.557	7.013
3	−5.4	4.988	6.946
4	−5.2	3.252	5.035
5	−5.1	3.181	5.055
6	−5.1	2.128	3.957
7	−4.9	4.194	6.630
8	−4.9	19.743	23.149
9	−4.8	26.463	29.416